arXiv:0712.2301v1 [astro-ph] 14 Dec 2007

Galaxy Orbits for Galaxy Clusters in Sloan Digital Sky Survey and 2dF Galaxy Redshift Survey

Ho Seong Hwang[1,2] and Myung Gyoon Lee[1]

`hshwang@kias.re.kr, mglee@astro.snu.ac.kr`

ABSTRACT

We present the results of a study for galaxy orbits in galaxy clusters using a spectroscopic sample of galaxies in Sloan Digital Sky Survey (SDSS) and 2dF Galaxy Redshift Survey (2dFGRS). We have determined the member galaxies of Abell clusters covered by these surveys using the galaxies' redshift and positional data. We have selected 10 clusters using three criteria: the number of member galaxies is greater than or equal to 40, the spatial coverage is complete, and X-ray mass profile is available in the literature. We derive the radial profile of the galaxy number density and velocity dispersion using all, early-type, and late-type galaxies for each cluster. We have investigated the galaxy orbits for our sample clusters with constant and variable velocity anisotropies over the clustercentric distance using Jeans equation. Using all member galaxies, the galaxy orbits are found to be isotropic within the uncertainty for most of sample clusters, although it is difficult to conclude strongly for some clusters due the large errors and the variation as a function of the clustercentric distance in the calculated velocity anisotropies. We investigated the orbital difference between early-type and late-type galaxies for four sample clusters, and found no significant difference between them.

Subject headings: galaxies: clusters: general – galaxies: clusters: individual (A85, A779, A1650, A1651, A1795, A1800, A2034, A2199, A2670, and A2734) – galaxies: kinematics and dynamics

---

[1] Astronomy Program, Department of Physics and Astronomy, Seoul National University, 56-1 Sillim 9-dong, Gwanak-gu, Seoul 151-742, Korea

[2] School of Physics, Korea Institute for Advanced Study, Seoul 130-722, Korea

1. Introduction

The mass estimate of a galaxy cluster, the largest gravitationally bounded system in the universe, was given for the first time by Zwicky (1933), which showed an indication of the existence of dark matter. In general, the cluster mass ranges from $10^{13} M_\odot$ for small groups to $10^{15} M_\odot$ for rich clusters, which is in the form of galaxies ($1 - 2\%$ of the total mass, e.g., Lin et al. 2003), hot X-ray emitting gas ($5 - 15\%$, e.g., Vikhlinin et al. 2006), dark matter ($80 - 90\%$) that affects the galaxy cluster through the gravitation only.

To determine the amount and distribution of underlying dark matter in clusters, Jeans analysis using the positional and velocity data of cluster galaxies has been usually adopted among several mass estimation methods (Katgert et al. 2004; Biviano 2006). However, previous studies had to assume the galaxy orbit in prior to derive the mass profile of galaxy clusters, due to the 'mass-orbit' degeneracy in the velocity dispersion profile (VDP) (e.g., Merritt 1987). This degeneracy can be broken by an orbit analysis with an independent mass determination based on X-ray or lensing studies, or by an analysis of higher order moments of velocity distribution : velocity dispersion and kurtosis (e.g., Łokas & Mamon 2003; Łokas et al. 2006), Gauss-Hermite moments (e.g., van der Marel et al. 2000; Katgert et al. 2004).

The analysis of galaxy orbits for clusters was made for the Coma cluster for the first time by Kent & Gunn (1982) who used about 300 galaxy velocities. They showed that the galaxy orbits in Coma can not be primarily radial, and a significant fraction of kinetic energy must be in tangential direction even at large radii. With an aid of large redshift surveys for cluster galaxies such as Canadian Network for Observational Cosmology (CNOC; Yee et al. 1996), ESO Nearby Abell Cluster Survey (ENACS; Katgert et al. 1996), and Cluster and Infall Region Nearby Survey (CAIRNS; Rines et al. 2003), extensive analysis for galaxy orbits in clusters has been performed. Carlberg et al. (1997a,b) analyzed 14 CNOC clusters at $z = 0.17 - 0.54$, and found that the galaxy orbits are isotropic or modest radial. van der Marel et al. (2000), using the same CNOC data, concluded that their best-fit model is close to isotropic. Rines et al. (2003) secured 15,000 galaxies in CAIRNS data, and concluded that the galaxy orbits in their ensemble cluster are also consistent with being isotropic.

On the other hand, the difference in galaxy orbits and in galaxy velocity dispersions among galaxy types provide important clues to understand the formation history of the cluster (Biviano & Katgert 2004; Goto 2005). Biviano et al. (1997) studied kinematic difference between emission-line galaxies (ELGs) and non-ELGs using ENACS data, and found that the VDP of ELGs is consistent with being radial, while that of non-ELGs is not. Adami et al. (1998), based on simple modelling of observed VDP for about 2000 galaxies in 40 regular clusters, reported that the orbits of ellipticals are mostly tangential in the cluster core and are nearly isotropic outside, while those of spirals are predominantly radial. Mahdavi et al. (1999) analyzed a sample of 20 galaxy groups from Center for Astrophysics redshift survey. They found that star-forming galaxies or ELGs have moderately radial orbits, while old or absorption-line galaxies isotropic orbits within the errors. Recently, Biviano & Katgert (2004), using the ENACS data, studied the galaxy orbits of all galaxy classes (the brightest ellipticals, other ellipticals together with S0, early-type spirals, late-type spirals, and irregulars) for the first time. They reported that the brightest ellipticals do not yield equilibrium solution, other ellipticals together with S0 have isotropic orbits as given in Katgert et al. (2004), and early spirals are consistent with isotropic orbits, while late spirals prefer radial orbits to isotropic orbits. In contrast, Ramirez & de Souza (1998), using nearby ($z < 0.055$) Abell clusters, concluded that the orbits of elliptical galaxies in clusters are close to radial, while those of spirals more tangential or isotropic. For nine intermediate ($z \sim 0.1 - 0.4$) CNOC cluster, Ramírez et al. (2000) obtained similar results to those of Ramirez & de Souza (1998): bulge-dominated galaxies have more eccentric orbits than disk-dominated galaxies do. The cause for the different results of Ramírez et al. compared with other studies is discussed in detail in van der Marel et al. (2000) and Biviano (2002).

Above results of galaxy orbits are based on a composite clusters prepared by combining data for disparate clusters that might have different formation histories. Although it is helpful to make the composite cluster in order to overcome problems of 1) a limited number of measured galaxy velocities per cluster and 2) an application of spherical Jeans equation to an asymmetric cluster, the composite cluster might be significantly different from any real cluster. In addition, previous studies were not based on the independent measurements of cluster mass profiles, but based on the optical galaxy data. These problems can be overcome. Natarajan & Kneib (1996) demonstrated the galaxy orbits can be constrained using an independently determined mass profile. For A2218, they used mass estimates derived by combining strong and weak lensing effects, and found evidence for an anisotropic core. Later, Benatov et al. (2006) extended the study of galaxy orbits to five clusters using mass estimates from X-ray data. They reported that the galaxies in five clusters have diverse orbits, and the orbital profiles in observed and simulated clusters appear to be different: simulated clusters show preferentially tangential orbits. However, they did not divide the galaxy sample into different types to investigate the orbital properties of different galaxy types.

Recently, galaxy redshift surveys such as the Sloan Digital Sky Survey (SDSS; York et al. 2000) and the 2dF Galaxy Redshift Survey (2dFGRS; Colless et al. 2001) have provided redshift data for large samples of galaxies. In addition, X-ray mass profiles for numerous clusters become available (Reiprich & Böhringer 2002; Sanderson et al. 2003; Demarco et al.

2003; Brownstein & Moffat 2006; Vikhlinin et al. 2006; Voigt & Fabian 2006). By identifying member galaxies in clusters using these redshift and positional data and adopting X-ray mass profiles, we can investigate the galaxy orbits in clusters for a large sample of galaxy clusters without making the composite cluster. We can also investigate the orbital properties for different galaxy types.

In this paper, we present the results of a study for the orbits of galaxies in galaxy clusters, using a spectroscopic sample of galaxies in SDSS and 2dFGRS and X-ray mass profiles in the literature. Section 2 describes the sample of galaxies and clusters used in this study. Radial profiles of galaxy number density and velocity dispersion are derived in §3. Analysis of the galaxy orbits and global kinematics are given in §4 and §5, respectively. Discussion and summary are given in §6 and §7, respectively. Throughout, we adopt cosmological parameters $h = 0.7$, $\Omega_\Lambda = 0.7$, and $\Omega_M = 0.3$.

2. Data

2.1. Galaxy Sample

We used data from the spectroscopic sample of galaxies in the Legacy survey of SDSS Sixth Data Release[1] (Strauss et al. 2007), and in the 2dFGRS Final Data Release (Colless et al. 2001). SDSS is one of the largest imaging and spectroscopic survey, which covers more than a quarter of the sky (York et al. 2000) using a dedicated, 2.5-meter telescope (Gunn et al. 2006) at Apache Point Observatory, New Mexico. The telescope is equipped with a wide-field drift-scanning mosaic CCD camera that can image 1.5 $\deg^2$ of sky at a time for imaging survey (Gunn et al. 1998), and a pair of fiber-fed spectrographs that can measure spectra more than 600 objects in a single observation with 3° field of view (Uomoto et al. 1999; Castander et al. 2001; Blanton et al. 2003). Extensive description of SDSS data products is given by York et al. (2000) and Stoughton et al. (2002), and we only give a brief summary of the SDSS data. The imaging survey is carried out with five broad bands (*ugriz*) centered at 3551, 4686, 6166, 7480, and 8932 Å (Fukugita et al. 1996). The magnitude limits of five bands for point sources are 22.0, 22.2, 22.2, 21.3, and 20.5, respectively. The calibration of data products from imaging survey is given by several authors: data reduction and photometry (Lupton et al. 2002), photometric calibration (Hogg et al. 2001; Smith et al. 2002; Ivezić et al. 2004; Tucker et al. 2006), and astrometric calibration (Pier et al. 2003). The spectroscopic survey obtains spectra covering 3800−9200 Å, with a wavelength resolution,

---

[1] Access to Data Release 6 can be found on the SDSS Web site (http://www.sdss.org/dr6).

$\lambda/\delta\lambda \sim 1800$. There are three kinds of spectroscopic targets: main galaxy sample, luminous red galaxies (LRG), and quasar. The main galaxy sample consists of the galaxies with r-band Petrosian magnitude $r_{\rm pet} \leq 17.77$, which are corrected for Galactic foreground reddening using Schlegel et al. (1998). The galaxies with r-band Petrosian half-light surface brightness $\mu_{50} > 24.5$ mag arcsec^{-2} are rejected; the number ratio of rejected galaxies to all galaxies is only $\sim 1\%$. In addition, the galaxies with $3''$ fiber magnitudes brighter than 15 magnitude in g or r, or brighter than 14.5 magnitude in i are rejected to avoid the problems of saturation and cross-talk in the spectrographs. A detailed description for main galaxy sample is presented in Strauss et al. (2002).

We used the main galaxy sample of 528,000 galaxies with measured velocities for this study. The median redshift for this spectroscopic sample is 0.11. The uncertainties of the redshift measurements are $\sim$30 km s^{-1}. A redshift confidence parameter (zConf) is assigned from 0 to 1 in the SDSS catalogs. We used only those galaxies with zConf ≥ 0.65.

2dFGRS is a spectroscopic survey for nearly 246,000 galaxies selected in the photographic $b_{\rm J}$ band from the APM galaxy catalog (Colless et al. 2001). The survey uses the Two-degree Field (2dF) multifibre spectrograph on the Anglo-Australian Telescope, which measure spectra about 400 objects in a single observation with 2° field of view (Lewis et al. 2002). The wavelength coverage of the spectra is 3600−8000 Å with a resolution of 9 Å. The spectroscopic targets are the galaxies with extinction corrected magnitude $b_{\rm J} < 19.45$. The survey coverage consists of two delination stripes and 100 random fields, which cover in total over 2000 deg^2. The median redshift for the sample of galaxies is similar to that of SDSS. A redshift quality parameter Q is assigned in the range 1−5. The redshift measurements with Q$\geq$3 are 98.4% reliable, and have an overall rms uncertainty of $\sim$85 km s^{-1}. We used only the galaxies with Q$\geq$3 in this study.

Since some galaxies are covered in both SDSS and 2dFGRS, we matched the galaxies found in SDSS with those in 2dFGRS to make a master catalog. The mean difference in radial velocity Δv $(= v_{\rm SDSS} - v_{\rm 2dFGRS})$ between the SDSS and 2dFGRS measurements for the 29,200 matched galaxies is estimated to be ~ 13 km s^{-1}. We corrected the SDSS velocities by this mean difference, and used the average value of the velocities measured in SDSS and in 2dFGRS for further analysis.

To investigate the difference of galaxy orbits among subsamples, we divide the galaxies into early-type and late-type galaxies using spectroscopic parameters provided by each survey. For 2dFGRS galaxies, η parameter, which is a linear combination of emission and absorption components within the spectrum derived from the Principal Component Analysis, is assigned to each galaxy (Madgwick et al. 2002). This parameter denotes the ratio of the present to the past star-formation activity in each galaxy. Madgwick et al. (2002)

showed that the η parameter correlates well with galaxy morphology using the Kennicutt Atlas (Kennicutt 1992) (see their Fig. 4). They reported that the galaxies with $\eta < -1.4$ are corresponding to E/S0 and Sa and those with $\eta > -1.4$ to Sb and Scd. Similarly, for SDSS galaxies, `eclass` parameter, which is a projection of the first three principal components of the spectrum, is assigned to each galaxy. This parameter has values from about -0.35 (corresponding to early-type galaxies) to 0.5 (late-types), which was used to classify SDSS galaxies (e.g., Bernardi et al. 2003, 2006). In Figure 1, we plot the `eclass` parameter in SDSS versus the η parameter in 2dFGRS in order to determine the `eclass` value corresponding to the division value of $\eta = -1.4$. It is seen that two parameters correlate well and the majority of galaxies are located around (η, `eclass`)=(-2.65,-0.135). We determined the relation equation between two parameters using the ordinary least-square bisector method (Isobe et al. 1990). The fit was done for the galaxies with $\eta < 1.1$ and `eclass`< 0.09.

$$\texttt{eclass}_{\rm SDSS} = 0.0631(\pm 0.0004)\ \eta_{\rm 2dFGRS} + 0.0244(\pm 0.0008) \tag{1}$$

This relation indicates that the division value of $\eta = -1.4$ in 2dFGRS is equivalent to that of `eclass`$=-0.0640$ in SDSS. Therefore, we classified the galaxies into early-type galaxies if (i) $\eta < -1.4$ when the galaxy is surveyed only in 2dFGRS, (ii) `eclass`< -0.0640 when the galaxy is surveyed only in SDSS, and (iii) `eclass`< -0.0640 and $\eta < -1.4$ when the galaxy is surveyed both in SDSS and 2dFGRS. The rest were classified into late-type galaxies. Some galaxies without estimation of η parameter ($\eta = -99.9$) were not used for the analysis of subsamples.

2.2. Cluster Sample and Galaxy Membership in Clusters

We used the Abell catalog of galaxy clusters (Abell et al. 1989) to identify cluster galaxies in the survey data. Among the Abell clusters, we selected those that have known spectroscopic redshifts in the NASA/IPAC Extragalactic Database (NED). Finally, we selected 731 and 230 clusters located within the survey regions of SDSS and 2dFGRS, respectively, as a sample of clusters for further analysis.

In order to determine the membership of galaxies in a cluster, we used the “shifting gapper” method of Fadda et al. (1996) as used also for the study of global rotation of galaxy clusters (Hwang & Lee 2007). In the plot of radial velocity versus clustercentric distance of galaxies for a given cluster, we selected the member galaxies using a velocity gap of 950 km $\rm s^{-1}$ and a distance bin of 0.2 Mpc shifting along the distance from the cluster center. We used a larger bin width if the number of galaxies in a bin was less than 15. We applied this method to the galaxies within the radius at which the distance between adjacent galaxies is larger than 0.1 Mpc. If there are no adjacent galaxies with > 0.1 Mpc, we stopped the procedure at the radius of 3.5 Mpc. We iterated the procedure until the number of cluster members is converged. Finally, we selected 113 galaxy clusters in which the number of member galaxies is greater than or equal to 40 for further analysis.

Since it is necessary to determine the galaxy orbits using cluster mass profiles from X-ray data, we selected 21 galaxy clusters whose X-ray mass profiles are available in the literature (e.g., Reiprich & Böhringer 2002; Sanderson et al. 2003; Demarco et al. 2003; Brownstein & Moffat 2006). Then, we rejected 9 clusters (A1775, 2052, 2063, 2142, 2147, 2244, 2255, 4038, and 4059) that appear to be in the stage of interacting or merging in the plot of galaxy velocity versus clustercentric distance, and 2 clusters (A119 and A1656) whose survey coverages are not complete. Although A85 was partially surveyed, we included it into our sample since the uncovered region is only the small outer region of the entire cluster. Finally, we obtained a sample of 10 clusters that will be used for investigating the galaxy orbits.

Table 1 lists our sample clusters with Abell identification, right ascension and declination, Bautz-Morgan (B-M) type, the survey in which the cluster is covered, the redshift derived in this study (the biweight location of Beers et al. 1990), the physical extent corresponding to one arcmin, and the velocity dispersion (the biweight scale of Beers et al. 1990) and the number of galaxies for all, early-type, and late-type galaxies. Our sample clusters are found from $z = 0.023$ to $z = 0.113$ and have 78−754 member galaxies. The number of early-types is usually larger than that of late-types in clusters, and eight clusters have B-M type of I or II. Figure 2 shows plots of radial velocity as a function of clustercentric distance of galaxies and the velocity distributions for the 10 clusters. In Figure 3, we show the spatial distribution of cluster galaxies with measured velocities. For most clusters, early-types are centrally concentrated, while late-types are not.

Since the presence of substructure in clusters can affect the determination of the VDPs and the galaxy number density profiles, it is necessary to secure the galaxy sample outside the substructure in order to determine the galaxy orbits properly. Therefore, we show, for our sample cluster, the distribution of δ that indicates local deviations from the systemic velocity ($v_{\rm sys}$) and dispersion (σ_p) of the entire cluster in Figure 4 (see §5.2 for the explanation of δ in detail). We selected the galaxies with $\delta \leq 2.0$ that are regarded as the galaxies in the cluster main body for the orbit analysis, and compared the results for the different choice of δ value in §6.2.

3. Observed Properties of Galaxy Clusters

3.1. X-ray Mass Profile

We present X-ray mass profiles for our sample clusters in Figure 5. It appears that mass profiles from various references agree well as a whole in each cluster. In Table 2, we list the X-ray luminosity and the parameters for the X-ray mass profile. The first and second columns give Abell identification and the X-ray luminosity, respectively. The third and fourth columns are β parameter and core radius (r_c) derived from the standard β-model of cluster gas density profile, respectively (e.g., Cavaliere & Fusco-Femiano 1976). The fifth and sixth columns are isothermal gas temperature (T_X) in Reiprich & Böhringer (2002), and central gas temperature [$T(0)$] in Sanderson et al. (2003), respectively. The seventh column gives the polytropic index (γ) used in equation (4), and final column gives the reference of these parameters adopted in this study. Then, the gravitational cluster mass $M_{\rm tot}(r)$ is determined under the assumption of hydrostatic equilibrium through the equation,

$$M_{\rm tot}(r) = -\frac{kT(r)r}{G\mu m_p}\left(\frac{{\rm d}\ \ln\rho(r)}{{\rm d}\ \ln r} + \frac{{\rm d}\ \ln T(r)}{{\rm d}\ \ln r}\right), \tag{2}$$

where k is the Boltzmann constant, G is the gravitational constant, μ ($= 0.61$) is the mean molecular weight, m_p is the proton mass. The gas density profile is given by,

$$\rho(r) = \rho(0)\left[1 + \left(\frac{r}{r_c}\right)^2\right]^{-\frac{3}{2}\beta}. \tag{3}$$

For the clusters in Reiprich & Böhringer (2002), we use isothermal gas temperature (T_X) as $T(r)$. For the clusters in Sanderson et al. (2003), we use non-isothermal gas temperature profile that is linked to the gas density via a polytropic equation of state,

$$T(r) = T(0)\left[1 + \left(\frac{r}{r_c}\right)^2\right]^{-\frac{3}{2}\beta(\gamma-1)}, \tag{4}$$

where γ is the polytropic index and r_c and β are as defined previously. For A2034, the X-ray mass profile is available in Demarco et al. (2003). However, they present a different form of gas density profile from the standard β-model, so those parameters were not included in Table 2.

It is worth noting that the X-ray mass profiles may not be well determined outside the outer significance radius of the cluster, r_X, because the X-ray source count drops below the Poissonian 1σ error at $r > r_X$ (Reiprich & Böhringer 2002). It is also noted that the Jeans equation may not be applicable beyond a radius of r_{200} (usually called virial radius), because the dynamical equilibrium of the cluster is not guaranteed at this region. Therefore, careful interpretation is needed beyond r_X and r_{200}. We draw the vertical lines at the radius of r_X and r_{200} in Figures 5, 11, 12, 13, 14, and 15. The radius r_{200} that contains an overdensity $200\rho_{\rm c}$ where $\rho_{\rm c}$ is the critical density of the Universe, is computed for each cluster using the equation in Carlberg et al. (1997a):

$$r_{200} = \frac{3^{1/2}\sigma_{\rm cl}}{10H(z)}, \tag{5}$$

where $\sigma_{\rm cl}$ is a velocity dispersion of the cluster and the Hubble parameter at z is $H^2(z) = H_0^2[\Omega_M(1+z)^3 + \Omega_k(1+z)^2 + \Omega_\Lambda]$ (Peebles 1993). Ω_M, Ω_k, and Ω_Λ are dimensionless density parameters.

3.2. Galaxy Number Density Profile

We derived the galaxy number density profile for each cluster using the member galaxies with $\delta \leq 2.0$ selected in §2.2. Since SDSS and 2dFGRS are magnitude limit surveys ($r_{\rm pet} <$ 17.77 for SDSS and $\rm b_J$ < 19.45 for 2dFGRS) and the spectroscopic sample of galaxies are nearly complete within the magnitude limit, we can derive the galaxy number density profile for each cluster using spectroscopically selected member galaxies.

We display the galaxy number density profiles of all, early-type, and late-type galaxies for each cluster in Figures 6 and 7. We de-projected the observed number density using the method in McLaughlin (1999), and fitted the de-projected density profile with those of Navarro et al. (1997, NFW) and Hernquist (1990), which are represented by,

$$\nu_{\rm g}(r) = \nu_0 (r/r_s)^{-1}(1+r/r_s)^{-\alpha}, \tag{6}$$

where $\nu_{\rm g}(r)$ is a three dimensional density profile of the cluster galaxies, r_s is a scale radius, and $\alpha = 2$ for the NFW profile and $\alpha = 3$ for the Hernquist profile. We also fitted the de-projected density profile with that of Kim et al. (2005, KEK05), which is derived from the isotropic and isothermal galaxy orbits in clusters under the NFW distribution of dark matter. It is represented by,

$$\nu_{\rm g}(r) = \nu_0 \left[\frac{(1+r/r_s)^{(r_s/r)}}{e}\right]^{\eta_g} \tag{7}$$

where the dimensionless parameter η_g is defined by

$$\eta_g \equiv \frac{2GM_0}{r_s\sigma_r^2}. \tag{8}$$

We used as a characteristic mass M_0, X-ray mass estimate shown in Figure 5 at a radius of r_{200}, and used as a one-dimensional velocity dispersion σ_r, observed velocity dispersion σ_p shown in Table 1.

The solid, dashed, and dot-dashed lines represent the projected best fit curves of the NFW, Hernquist, and KEK05 profiles, respectively. We did not fit the profiles that give unstable de-projection, and did not include them in Figures 6 and 7. For the clusters (A1650, 1651, and 2670) surveyed in both SDSS and 2dFGRS, we used one data set (2dFGRS for A1650 and A1651, SDSS for A2670) for deriving number density profile since the spatial coverage of SDSS or 2dFGRS is not complete depending on clusters. For A85, the fit was done using only the galaxies in the inner region ($R < 26'$) because of incomplete coverage (see Fig. 3).

The fitting results for our sample are summarized in Table 3. It is found that the scale radius r_s of late-types in all profiles is larger than that of the early-types, showing that the latter is more concentrated toward the cluster center than the former. The steeper density profile of early-types compared with late-types is a clear indication of the morphology-density relation (e.g., Dressler 1980).

To test the effect of the incompleteness of spectroscopic sample on the galaxy number density profiles, we investigate the color magnitude diagram of the galaxies in the photometric and spectroscopic samples. It is well known that optical colors of early-type galaxies are strongly correlate with absolute magnitudes (color-magnitude relation, CMR), in the sense that the brighter galaxies are likely to be redder than the fainter galaxies (Baum 1959; Faber 1973; Visvanathan & Sandage 1977). In Figure 8, we plot the $g - r$ versus r for the SDSS cluster galaxies and the $B_J - R_F$ versus R_F for the 2dFGRS cluster galaxies. The cluster galaxies within the $R_{max}/2$ from the cluster center selected in §2.2 are shown in company with the photometric sample of galaxies without measured velocities in the same region. R_{max} is the largest clustercentric distance of the member galaxies, and varies depending on clusters. It shows that the colors correlate well with the observed magnitudes. The linear fits derived from repeated one sigma clipping using early-type galaxies selected in §2.1 are overlaid. The average of the CMR slopes for our sample clusters is found to be -0.019 ± 0.006 for SDSS clusters and -0.037 ± 0.024 for 2dFGRS clusters, which is consistent with the results of previous studies based on the same data (De Propris et al. 2004; Hogg et al. 2004; Gallazzi et al. 2006; Aguerri et al. 2007). It appears that most bright ($r < 14$ mag) galaxies following the CMR in the photometric sample are selected as member galaxies, implying that the incompleteness of spectroscopic sample in the cluster center does not affect the determination of the projected galaxy number density in Figures 6 and 7.

3.3. Velocity Dispersion Profile

We present, in Figures 9 and 10, the VDPs for all, early-type, and late-type galaxies with $\delta \leq 2.0$ in each cluster. We computed the velocity dispersion of the galaxies lying within a bin with fixed radial width, $\Delta R = R_{max}/15$ for all galaxies and $\Delta R = R_{max}/5$ for the early-type and late-type galaxies as increasing the bin center by a fixed step width, $\delta R = R_{max}/40$. We stopped the calculation when the number of galaxies in a bin is less than 9, and used larger bin size if the number of computed dispersions in a cluster is less than five. We do not present the profiles for the subsample of the cluster whose final number of computed dispersions is less than five. The velocity dispersions for our sample cluster are not similar, but show diverse features. In addition, they are not always constant throughout the radius.

4. Galaxy Orbits in Clusters

If we assume spherical symmetry of a collisionless galaxy cluster, we can apply the Jeans equation in the absence of rotation to the dynamical analysis of the cluster. The spherical Jeans equation is

$$\frac{d}{dr}\left(\nu_{\rm g}(r)\sigma_r^2(r)\right) + \frac{2\,\beta_{\rm orb}(r)}{r}\,\nu_{\rm g}(r)\sigma_r^2(r) = -\nu_{\rm g}(r)\,\frac{GM_{\rm tot}(r)}{r^2}\ , \qquad (9)$$

where $\sigma_r(r)$ is the radial component of velocity dispersion, $\beta_{\rm orb}(r) \equiv 1 - \sigma_\theta^2(r)/\sigma_r^2(r)$ is the velocity anisotropy[2], G is the gravitational constant, and $M_{\rm tot}(r)$ is the total gravitating mass contained within a sphere of radius r (e.g. Binney & Tremaine 1987). $\sigma_\theta(r)$ is the tangential component of velocity dispersion that is equal to the azimuthal component, $\sigma_\phi(r)$, in the absence of cluster rotation. However, cluster rotation is not negligible in some clusters (Hwang & Lee 2007).

With an aid of independent determination of the cluster mass profile using X-ray data, we determine the velocity anisotropy (orbits) of cluster galaxies using two methods: (1) from the comparison of the calculated VDP using the Jeans equation with the measured VDP (e.g., Côté et al. 2001; Hwang et al. 2007), and (2) to calculate directly $\beta_{\rm orb}(r)$ using the Jeans equation (e.g., Natarajan & Kneib 1996; Benatov et al. 2006).

---

[2] It is noted that $\beta_{\rm orb}(r)$ is velocity anisotropy, while β is a parameter used for X-ray mass profile in §3.1.

4.1. Method 1

Our strategy to determine the velocity anisotropy of cluster galaxies is as follows: (1) With the galaxy number density profile, $\nu_{\rm g}(r)$, of all, early-type, and late-type galaxies and the mass profile, $M_{\rm tot}(r)$, in hand, assuming constant velocity anisotropy, $\beta_{\rm orb}$, over the radius in prior, we compute the theoretical projected VDP, $\sigma_p(R)$ and theoretical projected aperture VDP, $\sigma_{ap}(\leq R)$, using the Jeans equation; (2) From the comparison of these calculated VDPs with measured VDPs, we determine the velocity anisotropy of cluster galaxies.

We begin by deriving the theoretical projected dispersion profiles. The equation (9), spherical Jeans equation can be solved for the radial component of velocity dispersion, $\sigma_r(r)$:

$$\sigma_r^2(r) = \frac{1}{\nu_{\rm g}(r)} \exp\left(-\int \frac{2\beta_{\rm orb}}{r}\, dr\right) \left[\int_r^\infty \nu_{\rm g}\, \frac{GM_{\rm tot}}{x^2}\, \exp\left(\int \frac{2\beta_{\rm orb}}{x}\, dx\right) dx\right] . \tag{10}$$

Then the projected VDP, $\sigma_p(R)$ can be derived by

$$\sigma_p^2(R) = \frac{2}{\Sigma_{\rm g}(R)} \int_R^\infty \nu_{\rm g}\sigma_r^2(r) \left(1 - \beta_{\rm orb}\, \frac{R^2}{r^2}\right) \frac{r\, dr}{\sqrt{r^2 - R^2}}, \tag{11}$$

where R is the projected clustercentric distance, and $\Sigma_{\rm g}(R)$ is the projected density profile that is a projection of the three-dimensional density profile $\nu_{\rm g}(r)$:

$$\Sigma_{\rm g}(R) = 2\int_R^\infty \nu_{\rm g}(r) \frac{r\, dr}{\sqrt{r^2 - R^2}} \ . \tag{12}$$

The projected aperture dispersion profile, $\sigma_{ap}(\leq R)$, which is the velocity dispersion of all objects interior to a given projected radius R, can be computed by

$$\sigma_{\rm ap}^2(\leq R) = \left[\int_{R_{\rm min}}^R \Sigma_{\rm g}(R')\sigma_p^2(R')\, R'\, dR'\right] \left[\int_{R_{\rm min}}^R \Sigma_{\rm g}(R')\, R'\, dR'\right]^{-1} , \tag{13}$$

where $R_{\rm min}$ is the projected clustercentric distance of the innermost data point for the cluster galaxies.

For all galaxies in a cluster, we present the measured VDP compared with the calculated VDP for different velocity anisotropies in Figures 11, 12, and 13. The top panels show the projected VDPs, and the middle panels show the projected aperture VDPs. The measured dispersion data taken from Figures 9 and 10 are shown by filled circles along with their confidence intervals. The projected aperture dispersion profiles are plotted using a similar fashion to the case of the top panel. Although it is difficult to distinguish the velocity anisotropy clearly in the top panel (the middle panels show more stable result), it appears that the galaxy orbits in clusters show diverse patterns. Three results based on NFW, Hernquist, and KEK05 profiles of galaxy number density appear to be similar for a cluster. In Figures 14 and 15, we show the results of similar analysis for early-type and late-type galaxies, respectively. The difference between subsamples in a cluster is not clearly seen at this stage, and we discuss in detail the individual cluster in Appendix A.

4.2. Method 2

We combine the equation (9), spherical Jeans equation with the equation (11) that defines the projected VDP in order to compute $\beta_{\rm orb}(r)$ as a function of the radius directly.

Replacing $\beta_{\rm orb}$ in equation (11) with that in equation (9), we get,

$$\begin{aligned} &\frac{1}{2}\left[\, \Sigma_g(R)\ \sigma_p^2(R) -\ R^2\int_R^\infty \frac{GM_{\rm tot}(r)\nu_g}{r^2\sqrt{r^2-R^2}}\,dr\right] \\ =\ &\int_R^\infty \frac{r\nu_g\sigma_r^2 dr}{\sqrt{r^2-R^2}} + \frac{R^2}{2}\int_R^\infty \frac{d(\nu_g\sigma_r^2)}{dr}\frac{dr}{\sqrt{r^2-R^2}}. \end{aligned} \tag{14}$$

This equation can be reduced by integrating the second term on the right-hand side by parts (Binney & Mamon 1982),

$$\begin{aligned} &\frac{1}{2}\left[\Sigma_g(R)\sigma_p^2(R) - R^2\int_R^\infty \frac{GM_{\rm tot}(r)\nu_g}{r^2\sqrt{r^2-R^2}}dr\right] \\ &\qquad = \int_R^\infty \frac{(\frac{3R^2}{2}-r^2)}{\sqrt{r^2-R^2}}\frac{d(\nu_g\sigma_r^2)}{dr}\,dr. \end{aligned} \tag{15}$$

Then, $\nu_g\sigma_r^2$ can be expressed as a sum of four integrals (see Bicknell et al. 1989 for detail),

$$\nu_g(r)\sigma_r^2 = {\rm I}_1({\rm r}) - {\rm I}_2(r) + {\rm I}_3(r) - {\rm I}_4(r), \tag{16}$$

$${\rm I}_1(r) = \frac{1}{3}\int_r^\infty \frac{GM_{\rm tot}(r)\nu_g}{r^2}{\rm d}r, \tag{17}$$

$$\mathrm{I}_2(r) = \frac{2}{3r^3}\int_0^r GM_{\rm tot}(r)\nu_g r\mathrm{d}r, \tag{18}$$

$$\mathrm{I}_3(r) = \frac{1}{r^3}\int_0^r R\Sigma_g(R)\sigma_p^2(R)\mathrm{d}R, \tag{19}$$

$$\mathrm{I}_4(r) = \frac{2}{\pi r^3}\int_r^\infty R\Sigma_g(R)\sigma_p^2(R)\Big(\frac{r}{\sqrt{R^2-r^2}} - \sin^{-1}\frac{r}{R}\Big)\mathrm{d}R. \tag{20}$$

After computing $\nu_g\sigma_r^2$, we finally obtain $\beta_{\rm orb}(r)$ from the Jeans equation,

$$\beta_{\rm orb}(r) = -\frac{r}{2\nu_g\sigma_r^2}\Big[\frac{GM_{\rm tot}(r)\nu_g}{r^2} + \frac{\mathrm{d}}{\mathrm{d}r}(\nu_g\sigma_r^2)\Big]. \tag{21}$$

Practically, all integrations up to infinity were performed using a large radius, $R_t = 1.5R_{max}$ at which both $\nu_{\rm g}\sigma_r^2$ and $\Sigma_{\rm g}(R)$ approach to zero. In addition, input VDPs derived in §3.3 were smoothed for stable computation. We compute $\beta_{\rm orb}$ using the above equation, and present the results in the bottom panels of Figures 11, 12, and 13. The errors of $\beta_{\rm orb}$ are computed using the upper and lower confidence intervals of the VDPs shown in Figures 9 and 10. The behavior of $\beta_{\rm orb}$ computed in this Section is similar to that in §4.1. It is noted that the calculated $\beta_{\rm orb}$ may not be reliable in the very inner region where the observed VDPs are not available (interpolation of the observed VDPs in the outer region is used) and X-ray mass profiles are not properly determined due to the low resolution of X-ray instrument. Three results based on NFW, Hernquist, and KEK05 profiles of galaxy number density are also similar for a cluster. We also show the results of similar analysis for early-type and late-type galaxies in Figures 14 and 15, respectively. Detailed discussion of the individual cluster is given in Appendix A.

5. Global Cluster Properties

5.1. Cluster Morphology

In order to investigate the connection between cluster morphology and cluster dynamics, it is useful to determine the ellipticity and orientation of a cluster using the spatial distribution of the member galaxies. To determine the cluster shape, we employ the dispersion ellipse of the bivariate normal frequency function of position vectors (see, e.g., Trumpler & Weaver

1953; Carter & Metcalfe 1980; Burgett et al. 2004; Hwang & Lee 2007). The dispersion ellipse is defined by Trumpler & Weaver (1953) as the contour at which the density is 0.61 times the maximum density of a set of points distributed normally with respect to two correlated variables, although the points need not be distributed normally in order to determine the proper cluster shape. From the first five moments of the spatial distribution,

$$\mu_{10} = \frac{1}{N}\sum_{i=1}^{N} X_i, \quad \mu_{01} = \frac{1}{N}\sum_{i=1}^{N} Y_i \tag{22a}$$

$$\mu_{20} = \frac{1}{N}\sum_{i=1}^{N} X_i^2 - \left(\frac{1}{N}\sum_{i=1}^{N} X_i\right)^2 \tag{22b}$$

$$\mu_{11} = \frac{1}{N}\sum_{i=1}^{N} X_i Y_i - \frac{1}{N^2}\sum_{i=1}^{N} X_i \sum_{i=1}^{N} Y_i \tag{22c}$$

$$\mu_{02} = \frac{1}{N}\sum_{i=1}^{N} Y_i^2 - \left(\frac{1}{N}\sum_{i=1}^{N} Y_i\right)^2 \quad , \tag{22d}$$

where X and Y are clustercentric distances in the direction of right ascension and declination, respectively, the semimajor and semiminor axes of the ellipse, Γ_A and Γ_B, are derived by solving the equation

$$\begin{vmatrix} \mu_{20} - \Gamma^2 & \mu_{11} \\ \mu_{11} & \mu_{02} - \Gamma^2 \end{vmatrix} = 0 \quad . \tag{23}$$

The position angle of the major axis, measured from north to east, is given by

$$\Theta_2 = \cot^{-1}\left(-\frac{\mu_{02} - \Gamma_A^2}{\mu_{11}}\right) + \frac{\pi}{2} \quad , \tag{24}$$

and the ellipticity is defined by

$$\epsilon = 1 - \frac{\Gamma_B}{\Gamma_A} \quad . \tag{25}$$

The major and minor axes, position angles, and ellipticities derived for our sample clusters are listed in Table 4, and the dispersion ellipse is shown in Figure 3. The ellipticities are in the range $\epsilon = 0.15 - 0.36$, indicating no strong elongation.

5.2. Analysis of Substructure

The analysis of substructure is a useful diagnostic tool for understanding the dynamical state of galaxy clusters. A useful discussion of several substructure tests is given in Pinkney et al. (1996). As described in Hwang & Lee (2007), we derived number density maps using the spatial position (two-dimensional; 2D) of member galaxies, and performed one-dimensional (1D) and three-dimensional (3D) substructure tests for our sample clusters.

The majority of 1D (velocity histogram) substructure tests are normality tests. We present the results of five 1D tests in Table 5. The values of the I-test (Teague et al. 1990) are shown in the second and the third column; I_{90} is the critical value for rejecting the Gaussian hypothesis at 90% confidence. Therefore, a velocity distribution is considered to be non-Gaussian if $I > I_{90}$. We find that four of the sample clusters (A779, 1650, 1651, and 2199) do not satisfy the Gaussian hypothesis using the I test.

The skewness, which is a measure of the degree of asymmetry of a distribution, and the confidence level at which it rejects normality are given in the fourth and the fifth columns of Table 5. Positive or negative skewness indicates that the distribution is skewed to the right or left, respectively, with a longer tail to one side of the distribution maximum. The kurtosis, which is the degree to which a distribution is peaked, and the confidence level at which it rejects normality are given in the sixth and the seventh columns. Positive values indicate pointed or peaked distributions, while negative values indicate flattened or non peaked distributions. The skewness test rejects a Gaussian distribution with a confidence of over 90% for A85, 1651, and 2199. The kurtosis test rejects the hypothesis of Gaussianity for A779, 1650, 1651, 2034, and 2199 with confidence of over 90%.

From the eighth to the eleventh column of Table 5, we present the asymmetry index (AI) and the tail index (TI) introduced by Bird & Beers (1993) along with their confidence levels. The AI measures the symmetry in a population by comparing gaps in the data on the left and right sides of the sample median, and TI compares the spread of the data at the 90% level with the spread at the 75% level. The Gaussian hypothesis for A779, 1800, and 2199 are rejected by the AI test, and that for A85, 1650, 2199 by the TI test with a confidence level of over 90%.

We have constructed number density contours for the clusters using different bin sizes of $0.25R' \times 0.25R'$ Mpc^2 depending on the cluster size [$R' = 4(\Gamma_A \Gamma_B)^{1/2}/1.5$]. Γ_A and Γ_B are in units of Mpc, 4 is an arbitrary constant, and 1.5 (Mpc) is a normalization constant. We have smoothed the contours using a cubic convolution interpolation method. The contour interval, (max density in cluster)/6, is also determined according to the maximum number density of the clusters. We plot the number density contour map in the first and third columns of Figure 16.

Using the velocity data and positional information on the galaxies, we have performed a Δ-test (Dressler & Shectman 1988), which computes local deviations from the systemic velocity ($v_{\rm sys}$) and dispersion (σ_p) of the entire cluster. For each galaxy, the deviation is defined by

$$\delta^2 = \frac{N_{nn}}{\sigma_p^2}\left[(v_{\rm local} - v_{\rm sys})^2 + (\sigma_{\rm local} - \sigma_p)^2\right] \quad , \tag{26}$$

where N_{nn} is the number of galaxies that defines the local environment, taken to be $\sim {N_{gal}}^{1/2}$ in this study. The sum of δ over all galaxies in a cluster, Δ, is used to quantify the presence of substructure. It is approximately equal to the total number of galaxies in a cluster in the case of no substructure, while it is larger than the total number of galaxies in a cluster in the presence of substructure.

The statistical significance of the deviation is computed by Monte Carlo simulations. Velocities are randomly assigned to the galaxies at their observed positions, and $\Delta_{\rm sim}$ is computed for each simulated cluster. We construct 1000 simulated clusters and compute $\Delta_{\rm sim}$ for each simulation. We present $\Delta_{\rm obs}$ which is computed using real data and the fraction of simulated clusters with $\Delta_{\rm sim} > \Delta_{\rm obs}$ in the final two columns of Table 5. Small values of $f(\Delta_{\rm sim} > \Delta_{\rm obs})$ indicate statistically significant substructure. A779, 1795, 2199, and 2734 have much smaller values than other clusters, indicating significant substructures.

We plot the positions of cluster galaxies, represented by circles with radii proportional to e^δ, in the second and the fourth columns of Figure 16. A large circle denotes a galaxy that is deviant in either velocity or dispersion compared with nearby galaxies; therefore, groups of large circles indicate the presence of substructure. No strong substructures in A85, 1650, 1651, 1800, 2034, and 2670 were found with the $f(\Delta_{\rm sim} > \Delta_{\rm obs})$ test, as confirmed in Figure 16. In the number density contour maps of Figure 16, we present the galaxies with $\delta \leq 2.0$ that were used for orbit analysis (*dots*) and those with $\delta > 2.0$ in the substructure (*crosses*) separately, in order to show the usefulness of δ parameter to identify the substructure.

5.3. Dynamical Status of the Clusters

A study of the dynamical state for our sample clusters is useful for interpreting the galaxy orbits in clusters. It is expected from self-similar models that a relationship $L_{\rm x} \propto \sigma_p^4$ between the X-ray luminosity and the velocity dispersion of the clusters will exist (e.g. Quintana & Melnick 1982). For galaxy clusters in SDSS, Popesso et al. (2005) found $L_{\rm x} \propto$

$\sigma_p^{3.68\pm0.25}$. For galaxy clusters in 2dFGRS, Hilton et al. (2005) found a relation $L_{\rm x} \propto \sigma_p^{4.8\pm0.7}$ and suggested that high-$L_{\rm x}$ clusters are more dynamically evolved systems than the low-$L_{\rm x}$ clusters. In Figure 17, we plot the X-ray luminosity as a function of velocity dispersion and virial mass for our sample clusters (*filled circles*) for which X-ray luminosities are available in the literature, compared with other clusters (*open circles*) out of the 113 selected clusters. We plot the X-ray luminosities from different literature sources separately. It shows that $L_{\rm x}$ correlates well with σ_p and $M_{\rm vir}$. The power-law slopes are found to be in the range $3.7-4.9$ depending on X-ray references, which is consistent with the results of previous studies. Our sample clusters except for A779 are usually X-ray bright compared with the other clusters, because it is easy to derive X-ray mass profiles for the X-ray bright clusters. Interestingly, A779 and A1795 show a significant deviation from the relation $L_{\rm x}$-σ_p and $L_{\rm x}$-$M_{\rm vir}$.

The dynamics of the brightest cluster galaxies (BCGs) or cD galaxies in galaxy clusters are also useful for understanding the formation history of the clusters (see, e.g., Oegerle & Hill 2001). In particular, the peculiar velocity of the BCG, defined by $v_p = v_{BCG} - v_{\rm cl}$, where v_{BCG} is the observed velocity of BCGs and $v_{\rm cl}$ is the mean velocity of the cluster, is a useful indicator of the dynamical state of a cluster (Oegerle & Hill 2001). To estimate the peculiar velocities of BCGs in clusters, we first identified the BCGs that have the brightest $b_{\rm J}$ magnitudes in the catalog of member galaxies for the 113 selected galaxy clusters. Then we conducted a visual inspection of cluster images to determine whether there are any galaxies brighter than the selected BCGs, using the catalog of member galaxies. Since some very bright galaxies in clusters were not covered as a result of observational difficulties such as fiber collision and saturation, we finally selected 24 galaxy clusters for which the BCGs in the catalog agree with those in the images. Using this sample of 24 galaxy clusters, we plot, in Figure 18, the cluster velocity dispersion as a function of the absolute value of the BCG peculiar velocity, the absolute value of the BCG peculiar velocity as a function of clustercentric distance, and the redshift of the clusters as a function of the BCG absolute magnitude in the $b_{\rm J}$ band.

It appears that the absolute values of the peculiar velocities of the BCGs are in the range $5-802$ km s^{-1} and that the median value of the peculiar velocities is 165 km s^{-1}. The mean uncertainty on the values of the peculiar velocities is 117 km s^{-1}. In addition, the clustercentric distances of the BCGs are in the range $0-350$ kpc, and the median value of the clustercentric distances is 75 kpc. Interestingly, the BCG peculiar velocities for two (A1651 and A2670) clusters are larger than that median value, indicating dynamical non-equilibrium.

6. Discussion

We summarize the global kinematic properties for our sample clusters in Table 6. The first column gives the Abell identification. The second through fourth columns list the existence of substructure as indicated by the 1D, 2D, and 3D tests, respectively : “Yes” is assigned if three of five tests indicate the presence of substructure for 1D test, if the substructure at the contour level of 2×(max density in cluster)/6 is seen for 2D test, and if f($\Delta_{sim} > \Delta_{obs}$)$< 0.1$ for 3D test. The cluster morphology determined in §5.1 is given in the fifth column: “spherical” for ellipticity less than 0.2 and “elongated” for ellipticity greater than 0.2. “?” is given for A85 since the spatial coverage is incomplete. The dynamical status determined in §5.3 is given in the sixth and seventh columns. For the scaling relation between the X-ray luminosity and the velocity dispersion or the virial mass, “No” is assigned if the deviation of X-ray luminosities from the scaling relations derived in this study is larger than one standard deviation in at least four out of eight panels in Figure 17. For the peculiar velocities of the BCGs, “No” is assigned if the significance of the peculiar velocity of the BCG, S [$\equiv |v_p|/(\epsilon_{\rm BCG} + \epsilon_{\rm cl}^2)^{1/2}$], is larger than 3. $\epsilon_{\rm BCG}$ is the measurement error of the BCG velocity and $\epsilon_{\rm cl}$ is defined by $\epsilon_{\rm cl} \equiv \sigma_{\rm cl}^2/N_{gal}$, where $\sigma_{\rm cl}$ is the velocity dispersion of the cluster. The description on the result for the individual cluster is given Appendix A.

6.1. Effects of Different X-ray Mass Profiles

Since we used one X-ray mass profile per one cluster among several X-ray mass profiles, it is important to examine the results using different mass profiles. Moreover, the mass profile of Reiprich & Böhringer (2002) that we used in §3.1, adopted a constant gas temperature model to derive X-ray mass profile, but recent X-ray observations showed that gas temperature is not constant over the clustercentric distance (Markevitch et al. 1998; De Grandi & Molendi 2002; Pratt et al. 2007). The isothermal model is known to make the mass profile steeper than that of non-isothermal models, leading to underestimate the cluster mass at small radii and overestimate at large radii. Markevitch et al. (1998) showed that the isothermal model leads to underestimate the cluster mass by a factor of 0.74 of the non-isothermal model at one core radius and overestimate by a factor of 1.43 of the non-isothermal model at six core radius. To investigate the effects of different mass profiles on the determination of galaxy orbits, we compute $\beta_{\rm orb}$ in each cluster with various mass profiles, and present the results in Figure 19. The overestimation of the cluster mass from the isothermal model of Reiprich & Böhringer (2002) is expected to give larger value of calculated VDP than the true value, and the value of $\beta_{\rm orb}$ would decrease. Indeed it is seen that the cluster masses of the isothermal model in Reiprich & Böhringer (2002) are larger than those of non-isothermal model in Sanderson et al. (2003) at $r \sim r_{200}$ for A1651 and A2199 (Fig. 5). Therefore, the calculated $\beta_{\rm orb}$ with the isothermal model in Reiprich & Böhringer (2002) are smaller than those with the non-isothermal model Sanderson et al. (2003) [Fig. 19 (b) and (c)]. However, the orbit determination does not significantly change, because these values of $\beta_{\rm orb}$ with various mass profiles are not much different and accord within the uncertainty. It is noted that the galaxy orbits can be determined differently as seen in the case of A2199 (isotropic orbit for Sanderson et al. 2003, but tangential orbit for Markevitch et al. 1999 at $r \sim 0.35$ Mpc; see Appendix A.8).

The effect of the most accurate mass profile obtained with *Chandra* is seen in (d), (e), and (f). Since the *Chandra* mass profile is available for only A1795 and the discrepancy among the mass profiles in A1795 is not large, the calculated $\beta_{\rm orb}$ with *Chandra* mass profile appears to accord with those from other mass profiles within the uncertainty. The discrepancy becomes larger at large radius ($r > r_X$), but the reliability at this region is low because the mass profile is determined from the extrapolation of that for the inner region.

6.2. Effects of Different Galaxy Samples

Since significant fractions ($40 - 70\%$) of the clusters show substructures, indicating that they are in the process of merging (Jones & Forman 1999; Ramella et al. 2007), it is important to study the effect of the presence of substructure on the determination of galaxy orbits. It is expected that the presence of substructure leads to an increase of the observed VDP and the change of the galaxy number density profile. As a result, the orbit determination can be different depending on the degree of inclusion of the galaxies in the substructure. Previously, Biviano & Katgert (2004) showed that the galaxies in the substructure appear to have tangential orbit as a whole. Therefore, the orbit analysis including the galaxies in the substructure may make $\beta_{\rm orb}$ have low values.

Figure 20 shows the effect of the presence of substructure on the determination of galaxy orbits. As seen in (b)−(e), the calculated $\beta_{\rm orb}$ including the galaxies in the substructure (*dotted lines*) tends to be lower values than those excluding the galaxies in the substructure (*solid and dashed lines*), being compatible with the results of Biviano & Katgert (2004). However, A85 [Fig. 20 (a)] and late-type galaxies in A1795 [Fig. 20 (f)] do not show similar behavior to other cases, since the changes in observed VDPs and in galaxy number density profiles are not similar to other clusters. In conclusion, the orbit determination can be changed significantly [e.g., Fig 20 (f)], depending on the degree and the location of subclustering, but is not much changed for our sample clusters.

6.3. Comparison with the Previous Studies

For 10 Abell clusters, we have found that the orbits of galaxies are consistent with isotropic orbits in most clusters, although it is difficult to conclude strongly for some clusters due to the large errors (e.g., A779, A1650) and the variation as a function of clustercentric distance (e.g., A1795, A1800, A1795, A2199) in calculated $\beta_{\rm orb}$. Isotropic galaxy orbits for majority of our sample clusters, are consistent with those for composite clusters in the previous large cluster surveys (e.g., Carlberg et al. 1997a,b; van der Marel et al. 2000; Rines et al. 2003). Existence of anisotropic galaxy orbits is also reported in other studies. For A2218, Natarajan & Kneib (1996) found that the galaxy orbits are tangential at small radii ($R \leq 400$ kpc) and are radial at large radii. Benatov et al. (2006) analyzed the galaxy orbits for five clusters up to $r \sim r_{200}$, and reported that A2199 and A496 are consistent with tangential orbits, while A2390 radial orbits. Two clusters (MS1358 and A576) appear to have radial orbits, but these clusters may not be in hydrostatic equilibrium.

Numerical simulations showed that cluster galaxies are likely to follow isotropic orbits as seen in many clusters (e.g., Ghigna et al. 1998). In detail, isotropic orbits are preferred in the inner region, and radial orbits in the outer region, indicating existence of accreting galaxies from the cluster outskirt (Crone et al. 1994; Cole & Lacey 1996; Tormen et al. 1997; Thomas et al. 1998; Colín et al. 2000; Faltenbacher et al. 2005). However, tangential galaxy orbits found in the observational data, are not commonly seen in simulation data (Tormen et al. 1997; Thomas et al. 1998). Interestingly, Benatov et al. (2006) reported an offset in orbital profile for their observed and simulated clusters in the sense that the simulated clusters show preferentially tangential orbits.

For the orbital difference between early-type and late-type galaxies, the previous studies using the composite cluster, led to the conclusion that early-types have quasi-isotropic orbits and late-types radial orbits (Biviano et al. 1997; Mahdavi et al. 1999; Biviano & Katgert 2004). Interestingly, the clusters in which orbital difference among subsamples were studied in this study, show no significant difference between them. In order to investigate the origin of difference between this study and the previous studies, we show VDPs and projected galaxy number density profiles for several composite clusters in Figure 21. We construct the composite clusters for three different samples: Sample A - using four clusters in which orbital properties for subsamples are studied (A779, 1650, 1795, and 2199), Sample B - using six clusters in which orbital properties among subsamples are not studied (A85, 1651, 1800, 2034, 2670, and 2734), and Sample C - using 62 clusters without definite merging evidence, selected in §2.2. All samples are constructed using the galaxies outside the substructure ($\delta \leq 2.0$).

The VDP for the composite cluster is derived in the combined distribution of velocity relative to the cluster mean and normalized by the velocity dispersion of each cluster. It is known that the shape of VDP provides some hints for the galaxy orbits in clusters, and varies depending on clusters (den Hartog & Katgert 1996; Mahdavi et al. 1999; Muriel et al. 2002; Aguerri et al. 2007): flat, decaying, or rising VDP. It appears that the differences in VDPs and in projected galaxy number density profiles between early-type and late-type galaxies for Sample A are not significant at $0.3 < R/r_{200} < 0.8$ where the VDPs are available, while those in Sample B are large. In Sample C, the difference is significant with small errors: the values of velocity dispersion for late-types are larger than those for early-types, and the VDP for late-types is decreasing along the radius while that for early-types is nearly flat. Sample C is comparable to the composite cluster based on ENACS data used in Biviano & Katgert (2004), and our results for Sample C are similar to theirs. Thus, if we adopt the result of Katgert et al. (2004) that early-types have isotropic orbits, then the orbits for late-types in our composite cluster (Sample C) can be regarded as radial orbits, which is consistent with the results of the previous studies. Similarly, since not only VDPs but also projected galaxy number density profiles are not distinguishable in Sample A at $0.3 < R/r_{200} < 0.8$, it is expected that the orbital difference between early-type and late-type galaxies in Sample A is not significant. If we use the galaxies with lower probability of belonging to the substructure (e.g., $\delta \leq 1.4$), the results change little, indicating the effects of the galaxies substructure is not significant. Therefore, no orbital difference between early-type and late-type galaxies in Sample A can be interpreted as their own characteristics of individual clusters. Previously, Rines et al. (2005) also reported that the VDP of ELG is not different from the non-ELG for CAIRNS clusters, but their spatial distributions are different. In numerical simulations, Diaferio et al. (2001) found that there is no significant difference in orbital properties between red and blue galaxies : both red and blue galaxies are close to being isotropic. Thus, it is necessary to study what makes the diversity of galaxy orbits using more observational and simulation results.

7. Summary

We present the results of a study for the galaxy orbits in galaxy clusters using a spectroscopic sample of galaxies in SDSS and 2dFGRS. Our results are summarized as follows:

1. We have determined the member galaxies of 731 and 230 Abell clusters covered in SDSS and 2dFGRS, respectively. We have selected 10 clusters using three criteria : the number of member galaxies is greater than or equal to 40, the spatial coverage is complete, and X-ray mass profile is available in the literature.

2. For the selected 10 clusters, we derived the radial profile of the galaxy number density

and velocity dispersion for all, early-type, and late-type galaxies outside the substructure ($\delta \leq 2.0$).

3. We have investigated the galaxy orbits for our sample clusters with constant and variable $\beta_{\rm orb}$ through the clustercentric radius using Jeans equation. The resulting galaxy orbits based on two methods appear to be consistent.

4. Using all member galaxies, most of our sample clusters are found to be have isotropic orbits, although it is difficult to conclude strongly for some clusters due to the large errors (e.g., A779, A1650) and the variation as a function of clustercentric distance (e.g., A1795, A1800, A1795, A2199) in calculated $\beta_{\rm orb}$. For four clusters (A779, 1650, 1795, and 2199) the orbital difference between early-type and late-type galaxies appears not to be significant.

5. We have determined the cluster morphology using the dispersion-ellipse method, and have found the ellipticity in the range of $0.15 - 0.36$, indicating no strong elongation for our sample clusters.

6. We have investigated dynamical status for our sample clusters using substructure (1D, 2D, and 3D) tests, the relation between X-ray luminosity and the velocity dispersion or the virial mass, and peculiar velocity of BCGs. It is found that the majority of our sample clusters are dynamically relaxed system.

We thank the referee, A. Biviano, for useful comments that improved significantly the original manuscript. We also thank Woong-Tae Kim for useful comments on the galaxy number density profiles of clusters. We thank A.J.R. Sanderson and M. Markevitch for kindly providing us the central gas temperature data of our sample clusters. We also would like to thank all the people involved in creating the SDSS, 2dFGRS and NED. Funding for the SDSS and SDSS-II has been provided by the Alfred P. Sloan Foundation, the Participating Institutions, the National Science Foundation, the U.S. Department of Energy, the National Aeronautics and Space Administration, the Japanese Monbukagakusho, the Max Planck Society, and the Higher Education Funding Council for England. The SDSS Web Site is http://www.sdss.org. The SDSS is managed by the Astrophysical Research Consortium for the Participating Institutions. The Participating Institutions are the American Museum of Natural History, Astrophysical Institute Potsdam, the University of Basel, the University of Cambridge, Case Western Reserve University, the University of Chicago, Drexel University, Fermilab, the Institute for Advanced Study, the Japan Participation Group, Johns Hopkins University, the Joint Institute for Nuclear Astrophysics, the Kavli Institute for Particle Astrophysics and Cosmology, the Korean Scientist Group, the Chinese Academy of Sciences

(LAMOST), Los Alamos National Laboratory, the Max Planck Institute for Astronomy, the Max Planck Institute for Astrophysics, New Mexico State University, Ohio State University, the University of Pittsburgh, the University of Portsmouth, Princeton University, the US Naval Observatory, and the University of Washington. This research has made use of the NASA/IPAC Extragalactic Database (NED) which is operated by the Jet Propulsion Laboratory, California Institute of Technology, under contract with the National Aeronautics and Space Administration. This work was supported in part by grant R01-2004-000-10490-0 and R01-2007-000-20336-0 from the Basic Research Program of the Korea Science and Engineering Foundation.

A. Properties of Individual Clusters

A.1. Abell 85

A85 was covered in SDSS, but the outer region ($R > 26'$) was not surveyed (see Fig. 3). This cluster is in the complex of clusters Abell 85/87/89, and the member galaxies selected in this study include only Abell 85/87. The structure of this cluster is well studied by several authors (Lima Neto et al. 2001; Durret et al. 1998; Kempner et al. 2002; Durret et al. 2005): a southern blob (or group) that is merging from south ($\sim 10'$ from the cluster center), a subcluster that is merging from southwest ($\sim 4'$ from the cluster center), an extended 4 Mpc X-ray filament that is probably made of groups falling onto the main cluster. Interestingly, X-ray studies based on recent *Chandra* and XMM-Newton data (e.g., Kempner et al. 2002; Durret et al. 2005), provided an evidence of past and present merger activity for this cluster. Our galaxy data showed that only A87 ($\sim 30'$, or 1.9 Mpc from the southwest of the main cluster) is detected as a substructure, but some of the galaxies in A87 with $\delta \leq 2.0$ were removed for the orbit analysis. In addition, a small deviation from the scaling relation between X-ray and optical data and a small peculiar velocity of the BCG do not imply dynamical non-equilibrium. The galaxy orbits are consistent with isotropic orbits within the error at $0.3 < r < 1.5$ Mpc. Therefore, it appears that main cluster of A85 is stabilized at present, although it experienced a merging in the past, and is not disturbed significantly by the current merging event. We also find that the determined galaxy orbits do not change significantly, if we use different X-ray mass profiles as seen in Figure 19.

A.2. Abell 779

A779 is one of the nearest (z$\sim$0.023) clusters and shows the faintest X-ray luminosity in our sample. The velocity dispersion is the smallest ($\sigma_p = 491^{+40}_{-36}$ km s^{-1}) among our sample, and the number of late-types ($N_{gal} = 78$) is larger than that of early-types ($N_{gal} = 67$). This cluster has a cD galaxy, NGC 2832, which is known to be at rest in cluster potential (Oegerle & Hill 2001), but was not included in the spectroscopic sample of SDSS. The VDP using all member galaxies with $\delta \leq 2.0$ declines at $R \lesssim 0.8$ Mpc (see Fig. 9), which is consistent with the results of the previous studies (Mahdavi et al. 1999; Rines & Diaferio 2006). The galaxy orbits using all members appear to be consistent with radial or isotropic orbit within the uncertainty up to $r \sim r_{200}$, but it is difficult to conclude strongly due to the large error of calculated $\beta_{\rm orb}$. The orbits of early-types appear to be consistent with being radial or isotropic within the uncertainty through the radius, but strong conclusion is difficult due to the large error of calculated $\beta_{\rm orb}$. The orbits of late-types are consistent with being radial in the inner region ($r < 0.1$ Mpc) where the observed VDPs are not available, but with being isotropic within the error at $r < 1$ Mpc and become tangential at outer region.

A.3. Abell 1650

A1650 was included in both SDSS and 2dFGRS. A recent XMM-Newton observation showed no evidence for spatial temperature variation and surface brightness irregularity, indicating a relaxed system (Takahashi & Yamashita 2003). Similarly, we found no strong evidence for non-equilibrium (see Table 6). Figure 8 shows that $\rm B_J - R_F$ color of the BCG in this cluster is ~ 0.8 redder than the color expected from the CMR. However, this color deviation of the BCG in this cluster is not seen in other studies (Margoniner & de Carvalho 2000; Pimbblet et al. 2006). Therefore, the $\rm B_J - R_F$ color of the BCG given in 2dFGRS needs further investigation. The galaxy orbits for all member galaxies are found to be isotropic within the uncertainty or tangential at $r > 0.1$ Mpc. Interestingly, the orbits for early-type and late-type galaxies appear to be tangential at $r > 0.3$ Mpc.

A.4. Abell 1651

A1651 is included in both SDSS and 2dFGRS. This cluster is known to be a dynamically relaxed system: regular shape in the *ROSAT* PSPC image and symmetric temperature profile from *ASCA* data (Markevitch et al. 1998). Interestingly, a large peculiar velocity ($v_p = 350$

km s^{-1}) of the BCG is found in this study (see Fig. 18), indicating a dynamically unrelaxed system. Oegerle & Hill (2001) already identified a peculiar velocity of the BCG ($252 - 258$ km s^{-1}), but they concluded that the peculiar velocity is not large since a significance, S is less than 3. They obtained $S \sim 1.3$ with 39 member galaxies. However, we obtain $S = 3.46$ with a large number of member galaxies ($N_{gal} = 258$) and small velocity error, indicating a significant ($S > 3$) measured peculiar velocity. If we use the galaxies outside the substructure with $\delta \leq 2.0$, the result change little. This cluster was included in Las Campanas/Anglo-Australian Telescope Rich Cluster Survey (LARCS; Pimbblet et al. 2006), where a recession velocity of the cluster and the cD galaxy was determined to be 25466 ± 57 and 25571 ± 27 km s^{-1}, respectively. However, we obtain the mean velocity of the cluster (biweight location used in this study), $v_{\rm cl} = 25278 \pm 95$ km s^{-1} using their data, confirming significant peculiar velocity, $v_p = 293$ km s^{-1}. In contrast, the galaxy orbits are found to be isotropic within the uncertainty through the radius (see Fig. 11), which means that the galaxies are in equilibrium with the cluster potential, being consistent with the result from X-ray data. Therefore, it would be interesting to investigate what makes the large peculiar velocity of the BCG.

A.5. Abell 1795

A1795 is the most X-ray-luminous cluster in our sample. A cD galaxy in this cluster was not included in the spectroscopic sample of SDSS. A large peculiar velocity (365 km s^{-1}) of the cD galaxy was found by Hill et al. (1988), but later Oegerle & Hill (1994, 2001) reported the peculiar velocity is not large ($150 - 180$ km s^{-1}) and its significance is less than 3. Although detailed *Chandra* data showed that the central core of this cluster is not relaxed (e.g., Markevitch et al. 2001; Ettori et al. 2002; Fabian et al. 2001), other wide-field X-ray data indicate that the cluster is close to being dynamically relaxed (Briel & Henry 1996; Buote & Tsai 1996; Tamura et al. 2001). We found that the galaxy orbits derived from all member galaxies with $\delta \leq 2.0$ are consistent with being tangential at $0.3 < r < 1.2$ Mpc, but being isotropic within the uncertainty in the outer region. Interestingly, the orbits of early-types appear to be tangential at $r > 0.3$ Mpc, while those of late-types to be tangential or isotropic within the error. The results with different mass profiles are shown in Figure 19.

A.6. Abell 1800

A1800 is one of the member clusters in the Bootes supercluster (Einasto et al. 2001), and has a relatively small number ratio (~ 0.16) of late-types to early-types among our sample clusters. There is no strong evidence of dynamically non-equilibrium from the substructure tests and the scaling relation between X-ray and optical data. The galaxy orbits change from radial ($r < 0.2$ Mpc), to isotropic ($0.2 < r < 0.8$ Mpc) within the error and to tangential ($0.8 < r < 1.8$) Mpc.

A.7. Abell 2034

A2034 is the most distant cluster (z$\sim$ 0.113), and has the largest velocity dispersion (1208^{+80}_{-76} km s^{-1}) in our sample clusters. Interestingly, there are only four late-types out of 78 member galaxies. Since the observed VDP is larger than the upper envelope ($\beta_{\rm orb} = 0.99$) of the computed one over the radius, it is difficult to conclude using top and middle panels. However, the bottom panel indicates that the galaxy orbits are radial in the outer region ($r > 1$ Mpc), and those are consistent with isotropic orbits within the uncertainty at $0.2 < r < 1$ Mpc.

Larger values of observed VDP than the strong radial orbit can be interpreted as non-equilibrium of this cluster, although substructure tests and the scaling relation between X-ray and optical data in this study imply no strong substructure. However, other studies showed direct evidence of dynamical non-equilibrium. For example, detailed analysis of *Chandra* data revealed evidence for an ongoing merger (Kempner et al. 2003): northern cold front that is a discontinuity of the surface brightness on the northeast edge of the cluster, large concentration of galaxies including a cD galaxy just ahead of the cold front, and excess of emission to the south of cluster. In addition, a cD galaxy in the main cluster is offset $\sim 1'$ from the X-ray centroid. Unfortunately, the cD galaxy is not included in the spectroscopic sample of SDSS. If we adopt a receding velocity ($v_p = 33445 \pm 35$ km s^{-1}) of the cD galaxy in Miller et al. (2002), then the peculiar velocity for this galaxy is 477 ± 163 km s^{-1} with the significance of $S = 3.378$. This large peculiar velocity becomes larger if we use recession velocity ($v_{\rm cl} = 34373$ km s^{-1}) of the cluster determined in the same reference.

A.8. Abell 2199

The number of member galaxies ($N_{gal} = 754$) in A2199 is the largest among our sample clusters, and the number ($N_{gal} = 372$) of early-types is comparable to that ($N_{gal} = 382$) of late-types. A2199 is known to be one of the richest, regular cluster (Markevitch et al. 1999), and contains several infalling bound subclusters (Rines et al. 2001). Rines et al. (2002) derived the VDP up to 8 Mpc using $\sim$ 300 member galaxies in A2199, and found that the observed profile is consistent with an isotropic orbit based on the caustic mass profile. Łokas et al. (2006), using 180 member galaxies within $R \sim 1.1$ Mpc, determined $\beta_{\rm orb} = -0.55^{+1.05}_{-2.75}$ based on the joint analysis of velocity dispersion and kurtosis, which is consistent with a tangential or isotropic orbit. We found, using an independent X-ray mass profile and a smoothed velocity profile, that the galaxy orbits are isotropic at $0.1 < r < 0.7$ Mpc within the error, and are radial in the outer region. However, Benatov et al. (2006) found that A2199 has tangentially anisotropic orbit in the inner region ($R < 1.1$ Mpc), using an X-ray mass profile of Markevitch et al. (1999) and polynomial fit of VDP. This discrepancy is demonstrated in Figure 19 (c), and is because the mass profile of Markevitch et al. (1999) they used is larger than that we used (Sanderson et al. 2003) (see §6 for more detail). We also investigated the orbital difference between early-type and late-type galaxies in A2199. Interestingly, both subsamples appear to have radial through the radius, indicating they infall from the outer region.

A.9. Abell 2670

Abell 2670 was included in both SDSS and 2dFGRS. We found no strong evidence of substructure from the substructure tests, but identified a large peculiar velocity of the BCG, which was already found by Bird (1994a). Although X-ray morphology seen by *ROSAT* is regular, indicating a relaxed system (Hobbs & Willmore 1997), Bird (1994b) concluded that this cluster may consist of four subclusters that are merging along the line of sight, using ~ 230 galaxies in Sharples et al. (1988) catalog. Hobbs & Willmore (1997) also suggested a merging activity since the observed VDP is much greater than that expected from the X-ray mass profile. In contrast, we found isotropic galaxy orbits, which imply a relaxed system. The observed dispersion profile in this study is not significantly different from that in Hobbs & Willmore (1997). However, X-ray mass profiles adopted in this study are larger than that used in Hobbs & Willmore (1997), thus the value of expected dispersion is larger than that in Hobbs & Willmore (1997). Therefore, other evidence (e.g., irregular gas temperature map) is needed to confirm the merging activity of this cluster.

A.10. Abell 2734

Burgett et al. (2004) found no strong substructure using 125 velocity data from the 2dFGRS data. Similar results were found by other authors: Solanes et al. (1999) and Biviano et al. (2002) identified no substructure using 45 and 77 member galaxies in ENACS data, respectively. However, our 3D substructure test resulted in a strong substructure in this cluster. It is due to the larger spatial coverage than previous studies, therefore, the substructure at $R \sim 30'$ (~ 2 Mpc) to the south-east is included in this study. Comparison of *ROSAT* X-ray image with the optical one also shows a good agreement (Kolokotronis et al. 2001). den Hartog & Katgert (1996) derived a flat VDP up to R$\sim$ 1.5 Mpc using 77 velocity data in ENACS. The galaxy orbits appear to be isotropic within the uncertainty through the radius, indicating a dynamical equilibrium, which is consistent with the previous studies.

REFERENCES

Abell G. O., Corwin H. G., & Olowin R. P., 1989, ApJS, 70, 1

Adami, C., Biviano, A., & Mazure, A. 1998, A&A, 331, 439

Aguerri, J. A. L., Sánchez-Janssen, R., & Muñoz-Tuñón, C. 2007, A&A, 471, 17

Baum, W. A. 1959, PASP, 71, 106

Beers T. C., Flynn K., & Gebhardt K., 1990, AJ, 100, 32

Benatov, L., Rines, K., Natarajan, P., Kravtsov, A., & Nagai, D. 2006, MNRAS, 370, 427

Bernardi, M., et al. 2003, AJ, 125, 1817

Bernardi, M., Nichol, R. C., Sheth, R. K., Miller, C. J., & Brinkmann, J. 2006, AJ, 131, 1288

Bicknell, G. V., Bruce, T. E. G., Carter, D., & Killeen, N. E. B. 1989, ApJ, 336, 639

Binney, J., & Mamon, G. A. 1982, MNRAS, 200, 361

Binney, J., & Tremaine, S. 1987, Galactic Dynamics (Princeton: Princeton Univ. Press)

Bird C. M., & Beers, T. C. 1993, AJ, 105, 1596

Bird, C. M. 1994a, AJ, 107, 1637

Bird, C. 1994b, ApJ, 422, 480

Biviano, A., Katgert, P., Mazure, A., Moles, M., den Hartog, R., Perea, J., & Focardi, P. 1997, A&A, 321, 84

Biviano, A. 2002, Tracing Cosmic Evolution with Galaxy Clusters, 268, 127

Biviano, A., Katgert, P., Thomas, T., & Adami, C. 2002, A&A, 387, 8

Biviano, A., & Katgert, P. 2004, A&A, 424, 779

Biviano, A. 2006, XXVIth Astrophysics Moriond Meeting: "From dark halos to light", ed. L. Tresse, S. Maurogordato and J. Tran Thanh Van, (astro-ph/0607040)

Blanton, M. R., Lin, H., Lupton, R. H., Maley, F. M., Young, N., Zehavi, I., & Loveday, J. 2003, AJ, 125, 2276

Böhringer H., et al., 2000, ApJS, 129, 435

Böhringer H., et al., 2004, A&A, 425, 367

Briel, U. G., & Henry, J. P. 1996, ApJ, 472, 131

Brownstein, J. R., & Moffat, J. W. 2006, MNRAS, 367, 527

Buote, D. A., & Tsai, J. C. 1996, ApJ, 458, 27

Burgett W. S., et al., 2004, MNRAS, 352, 605

Carlberg, R. G., Yee, H. K. C., & Ellingson, E. 1997a, ApJ, 478, 462

Carlberg, R. G., et al. 1997b, ApJ, 485, L13

Carter D., & Metcalfe N., 1980, MNRAS, 191, 325

Castander, F. J., et al. 2001, AJ, 121, 2331

Cavaliere, A., & Fusco-Femiano, R. 1976, A&A, 49, 137

Colless M. et al., 2001, MNRAS, 328, 1039

Cole, S., & Lacey, C. 1996, MNRAS, 281, 716

Colín, P., Klypin, A. A., & Kravtsov, A. V. 2000, ApJ, 539, 561

Côté, P., et al. 2001, ApJ, 559, 828

Crone, M. M., Evrard, A. E., & Richstone, D. O. 1994, ApJ, 434, 402

De Grandi, S., & Molendi, S. 2002, ApJ, 567, 163

De Propris, R., et al. 2004, MNRAS, 351, 125

Demarco, R., Magnard, F., Durret, F., & Márquez, I. 2003, A&A, 407, 437

den Hartog R., & Katgert P., 1996, MNRAS, 279, 349

Diaferio, A., Kauffmann, G., Balogh, M. L., White, S. D. M., Schade, D., & Ellingson, E. 2001, MNRAS, 323, 999

Dressler, A. 1980, ApJ, 236, 351

Dressler A., & Shectman S. A., 1988, AJ, 95, 985

Durret, F., Forman, W., Gerbal, D., Jones, C., & Vikhlinin, A. 1998, A&A, 335, 41

Durret, F., Lima Neto, G. B., & Forman, W. 2005, A&A, 432, 809

Ebeling, H., Edge, A. C., Bohringer, H., Allen, S. W., Crawford, C. S., Fabian, A. C., Voges, W., & Huchra, J. P. 1998, MNRAS, 301, 881

Ebeling H., Edge A. C., Allen S. W., Crawford C. S., Fabian A. C., & Huchra J. P., 2000, MNRAS, 318, 333

Einasto M., Einasto J., Tago E., Müller V., & Andernach, H., 2001, AJ, 122, 2222

Ettori, S., Fabian, A. C., Allen, S. W., & Johnstone, R. M. 2002, MNRAS, 331, 635

Faber, S. M. 1973, ApJ, 179, 731

Fabian, A. C., Sanders, J. S., Ettori, S., Taylor, G. B., Allen, S. W., Crawford, C. S., Iwasawa, K., & Johnstone, R. M. 2001, MNRAS, 321, L33

Fadda D., Girardi M., Giuricin G., Mardirossian F., & Mezzetti M., ApJ, 473, 670

Faltenbacher, A., Kravtsov, A. V., Nagai, D., & Gottlöber, S. 2005, MNRAS, 358, 139

Fukugita, M., Ichikawa, T., Gunn, J. E., Doi, M., Shimasaku, K., & Schneider, D. P. 1996, AJ, 111, 1748

Gallazzi, A., Charlot, S., Brinchmann, J., & White, S. D. M. 2006, MNRAS, 370, 1106

Ghigna, S., Moore, B., Governato, F., Lake, G., Quinn, T., & Stadel, J. 1998, MNRAS, 300, 146

Goto, T. 2005, MNRAS, 359, 1415

Gunn, J. E., et al. 1998, AJ, 116, 3040

Gunn, J. E., et al. 2006, AJ, 131, 2332

Hilton, M., et al. 2005, MNRAS, 363, 661

Hernquist, L. 1990, ApJ, 356, 359

Hill, J. M., Hintzen, P., Oegerle, W. R., Romanishin, W., Lesser, M. P., Eisenhamer, J. D., & Batuski, D. J. 1988, ApJ, 332, L23

Hobbs, I. S., & Willmore, A. P. 1997, MNRAS, 289, 685

Hogg, D. W., Finkbeiner, D. P., Schlegel, D. J., & Gunn, J. E. 2001, AJ, 122, 2129

Hogg, D. W., et al. 2004, ApJ, 601, L29

Hwang, H. S., & Lee, M. G. 2007, ApJ, 662, 236

Hwang, H. S., et al. 2007, ApJ, in press (astro-ph/0709.4309)

Isobe, T., Feigelson, E. D., Akritas, M. G., & Babu, G. J. 1990, ApJ, 364, 104

Ivezić, Ž., et al. 2004, Astronomische Nachrichten, 325, 583

Jones C., & Forman W., 1999, ApJ, 511, 65

Katgert, P., et al. 1996, A&A, 310, 8

Katgert, P., Biviano, A., & Mazure, A. 2004, ApJ, 600, 657

Kempner, J. C., Sarazin, C. L., & Ricker, P. M. 2002, ApJ, 579, 236

Kempner, J. C., Sarazin, C. L., & Markevitch, M. 2003, ApJ, 593, 291

Kennicutt, R. C., Jr. 1992, ApJS, 79, 255

Kent, S. M., & Gunn, J. E. 1982, AJ, 87, 945

Kim, W.-T., El-Zant, A. A., & Kamionkowski, M. 2005, ApJ, 632, 157

Kolokotronis, V., Basilakos, S., Plionis, M., & Georgantopoulos, I. 2001, MNRAS, 320, 49

Ledlow M. J., Voges W., Owen F. N., & Burns J. O., 2003, AJ, 126, 2740

Lewis, I. J., et al. 2002, MNRAS, 333, 279

Lima Neto, G. B., Pislar, V., & Bagchi, J. 2001, A&A, 368, 440

Lin, Y.-T., Mohr, J. J., & Stanford, S. A. 2003, ApJ, 591, 749

Łokas, E. L., & Mamon, G. A. 2003, MNRAS, 343, 401

Łokas, E. L., Wojtak, R., Gottlöber, S., Mamon, G. A., & Prada, F. 2006, MNRAS, 367, 1463

Lupton, R. H., Ivezic, Z., Gunn, J. E., Knapp, G., Strauss, M. A., & Yasuda, N. 2002, Proc. SPIE, 4836, 350

Madgwick, D. S., et al. 2002, MNRAS, 333, 133

Mahdavi, A., Geller, M. J., Böhringer, H., Kurtz, M. J., & Ramella, M. 1999, ApJ, 518, 69

Margoniner, V. E., & de Carvalho, R. R. 2000, AJ, 119, 1562

Markevitch, M., Forman, W. R., Sarazin, C. L., & Vikhlinin, A. 1998, ApJ, 503, 77

Markevitch, M., Vikhlinin, A., Forman, W. R., & Sarazin, C. L. 1999, ApJ, 527, 545

Markevitch, M., Vikhlinin, A., & Mazzotta, P. 2001, ApJ, 562, L153

McLaughlin, D. E. 1999, AJ, 117, 2398

Merritt, D. 1987, ApJ, 313, 121

Miller, C. J., Krughoff, K. S., Batuski, D. J., & Hill, J. M. 2002, AJ, 124, 1918

Muriel, H., Quintana, H., Infante, L., Lambas, D. G., & Way, M. J. 2002, AJ, 124, 1934

Natarajan, P., & Kneib, J.-P. 1996, MNRAS, 283, 1031

Navarro, J. F., Frenk, C. S., & White, S. D. M. 1997, ApJ, 490, 493

Oegerle, W. R., & Hill, J. M. 1994, AJ, 107, 857

Oegerle, W. R., & Hill, J. M. 2001, AJ, 122, 2858

Peebles, P. J. E. 1993, Princeton Series in Physics, Princeton, NJ: Princeton University Press

Pier, J. R., Munn, J. A., Hindsley, R. B., Hennessy, G. S., Kent, S. M., Lupton, R. H., & Ivezić, Ž. 2003, AJ, 125, 1559

Pimbblet, K. A., Smail, I., Edge, A. C., O'Hely, E., Couch, W. J., & Zabludoff, A. I. 2006, MNRAS, 366, 645

Pinkney J., Roettiger K., Burns J. O., & Bird C. M., 1996, ApJS, 104, 1

Popesso, P., Biviano, A., Böhringer, H., Romaniello, M., & Voges, W. 2005, A&A, 433, 431

Pratt, G. W., Böhringer, H., Croston, J. H., Arnaud, M., Borgani, S., Finoguenov, A., & Temple, R. F. 2007, A&A, 461, 71

Quintana, H., & Melnick, J. 1982, AJ, 87, 972

Ramella, M., et al. 2007, A&A, 470, 39

Ramirez, A. C., & de Souza, R. E. 1998, ApJ, 496, 693

Ramírez, A. C., de Souza, R. E., & Schade, D. 2000, ApJ, 533, 62

Reiprich, T. H., Böhringer, H. 2002, ApJ, 567, 716

Rines, K., Mahdavi, A., Geller, M. J., Diaferio, A., Mohr, J. J., & Wegner, G. 2001, ApJ, 555, 558

Rines, K., Geller, M. J., Diaferio, A., Mahdavi, A., Mohr, J. J., & Wegner, G. 2002, AJ, 124, 1266

Rines, K., Geller, M. J., Kurtz, M. J., & Diaferio, A. 2003, AJ, 126, 2152

Rines, K., Geller, M. J., Kurtz, M. J., & Diaferio, A. 2005, AJ, 130, 1482

Rines, K., & Diaferio, A. 2006, AJ, 132, 1275

Sanderson, A. J. R., Ponman, T. J., Finoguenov, A., Lloyd-Davies, E. J., & Markevitch, M. 2003, MNRAS, 340, 989

Schlegel, D. J., Finkbeiner, D. P., & Davis, M. 1998, ApJ, 500, 525

Sharples, R. M., Ellis, R. S., & Gray, P. M. 1988, MNRAS, 231, 479

Smith, J. A., et al. 2002, AJ, 123, 2121

Solanes, J. M., Salvador-Solé, E., & González-Casado, G. 1999, A&A, 343, 733

Stoughton, C., et al. 2002, AJ, 123, 485

Strauss, M. A., et al. 2002, AJ, 124, 1810

Strauss, M. A., et al. 2007, ApJ, in press

Takahashi, S., & Yamashita, K. 2003, PASJ, 55, 1105

Tamura, T., et al. 2001, A&A, 365, L87

Teague P. F., Carter D., & Gray P. M., 1990, ApJS, 72, 715

Thomas, P. A., et al. 1998, MNRAS, 296, 1061

Tormen, G., Bouchet, F. R., & White, S. D. M. 1997, MNRAS, 286, 865

Trumpler R. J., & Weaver H. F., 1953, Statistical Astronomy (Univ. California Press, Berkeley)

Tucker, D. L., et al. 2006, Astronomische Nachrichten, 327, 821

Uomoto, A., et al. 1999, Bulletin of the American Astronomical Society, 31, 1501

van der Marel, R. P., Magorrian, J., Carlberg, R. G., Yee, H. K. C., & Ellingson, E. 2000, AJ, 119, 2038

Vikhlinin, A., Kravtsov, A., Forman, W., Jones, C., Markevitch, M., Murray, S. S., & Van Speybroeck, L. 2006, ApJ, 640, 691

Visvanathan, N., & Sandage, A. 1977, ApJ, 216, 214

Voigt, L. M., & Fabian, A. C. 2006, MNRAS, 368, 518

Yee, H. K. C., Ellingson, E., & Carlberg, R. G. 1996, ApJS, 102, 269

York D. G. et al., 2000, AJ, 120, 1579

Zwicky, F. 1933, Helvetica Physica Acta, 6, 110

This preprint was prepared with the AAS LaTeX macros v5.2.

Table 1. The Sample of Galaxy Clusters

							All		Early-types		Late-types	
Cluster	R.A. (J2000)	Decl. (J2000)	B-M Type	Survey[a]	$\overline{cz}$ (km s^{-1})	kpc/arcmin	σ_p (km s^{-1})	N_{gal}	σ_p (km s^{-1})	N_{gal}	σ_p (km s^{-1})	N_{gal}
A0085	00 41 50.09	−09 18 06.8	I	S	16545^{+65}_{-64}	64.3	926^{+57}_{-51}	208	804^{+61}_{-54}	170	1114^{+108}_{-109}	38
A0779	09 19 41.28	+33 45 46.8	I-II	S,2	6947^{+41}_{-39}	28.1	491^{+40}_{-36}	145	471^{+73}_{-68}	67	479^{+47}_{-40}	78
A1650	12 58 41.09	−01 45 24.8	I-II	S,2	25187^{+46}_{-46}	94.7	762^{+39}_{-39}	258	722^{+51}_{-49}	168	829^{+65}_{-60}	89
A1651	12 59 21.50	−04 11 40.9	I-II	S	25222^{+55}_{-55}	94.8	881^{+46}_{-44}	258	828^{+56}_{-51}	169	996^{+90}_{-79}	84
A1795	13 48 52.97	+26 35 44.2	I	S	18775^{+67}_{-62}	72.4	755^{+43}_{-39}	163	729^{+49}_{-45}	127	806^{+70}_{-80}	36
A1800	13 49 21.65	+28 06 13.0	II	S	22660^{+87}_{-85}	86.0	762^{+49}_{-45}	93	722^{+45}_{-45}	80	786^{+184}_{-196}	13
A2034	15 10 11.74	+33 30 52.9	II-III	S	33922^{+160}_{-156}	123.3	1208^{+80}_{-76}	78	1185^{+67}_{-69}	74	1746^{+742}_{-1006}	4
A2199	16 28 37.97	+39 32 55.3	I	S	9221^{+28}_{-29}	36.9	726^{+22}_{-20}	754	703^{+30}_{-29}	372	750^{+31}_{-30}	382
A2670	23 54 13.39	−10 24 46.1	I-II	S,2	22837^{+84}_{-82}	86.6	844^{+51}_{-49}	106	840^{+59}_{-56}	82	870^{+100}_{-104}	24
A2734	00 11 20.71	−28 51 18.0	III	2	18256^{+81}_{-76}	70.5	1001^{+52}_{-51}	192	831^{+70}_{-67}	120	1175^{+82}_{-79}	68

[a] 'S' is covered by SDSS and '2' by 2dFGRS.

Table 2: X-ray Properties for Our Sample Clusters

Cluster	$L_{\rm x}$(0.1–2.4 keV)[a] (10^{44} ergs cm^{-2} s^{-1})	β	r_c (kpc)	T_X (keV)	$T(0)$ (keV)	γ	Ref.[b]
A0085	9.789	0.76	293.8	...	10.97	1.32	S03
A0779	0.090	0.34	39.4	...	3.66	1.02	S03
A1650	7.308	0.78	214.2	...	9.73	1.19	S03
A1651	8.000	0.70	192.5	...	6.87	1.10	S03
A1795	10.124	0.83	288.4	...	9.98	1.17	S03
A1800	2.840	0.77	280.0	4.02	...	...	R02
A2034	6.850	...	...	...	...	...	D03
A2199	4.165	0.60	76.9	...	4.17	1.15	S03
A2670	1.469	0.55	83.8	...	5.99	1.04	S03
A2734	2.365	0.62	151.4	3.85	...	...	R02

[a] A0779 (Ebeling et al. 2000), A2034 (Ebeling et al. 1998), A2670 (Böhringer et al. 2004), & other clusters (Reiprich & Böhringer 2002).

[b] R02 (Reiprich & Böhringer 2002), S03 (Sanderson et al. 2003), and D03 (Demarco et al. 2003).

Table 3. Galaxy Number Density Profile for the Clusters

Cluster	$\nu_{0,\rm NFW}$ (arcmin^{-3})	$r_{s,\rm NFW}$ (arcmin)	$\nu_{0,\rm Her}$ (arcmin^{-3})	$r_{s,\rm Her}$ (arcmin)	$\nu_{0,\rm KEK05}$ (arcmin^{-3})	$r_{s,\rm KEK05}$ (arcmin)	$\eta_{g,\rm KEK05}$
All Galaxies							
A0085	$1.34E-3$	30.2	$6.85E-4$	54.6	$1.79E-2$	15.6	9.0
A0779	$8.82E-3$	7.4	$8.01E-4$	29.1	$2.05E-2$	16.0	12.7
A1650	$4.33E-3$	15.3	$1.59E-3$	33.6	$4.14E-2$	13.0	10.7
A1651	$3.95E-3$	15.3	$1.86E-3$	30.1	$4.67E-2$	10.4	10.1
A1795	$3.88E-3$	13.7	$1.69E-3$	28.4	$2.83E-2$	16.4	11.8
A1800	$7.88E-3$	8.0	$2.99E-3$	17.6	$5.96E-2$	9.0	11.5
A2034	$1.88E-2$	6.3	$6.89E-3$	14.0	$1.47E-1$	6.3	11.1
A2199	$5.33E-4$	40.5	$1.56E-4$	98.1	$8.07E-3$	23.3	9.9
A2670	$3.43E-3$	15.6	$1.61E-3$	29.7	$2.66E-2$	10.9	9.1
A2734	$2.35E-2$	5.6	$6.81E-3$	14.4	$1.52E-1$	6.6	11.7
Early-type Galaxies							
A0779	$7.73E-2$	2.3	$1.26E-3$	17.3	$1.22E-2$	16.1	13.6
A1650	$9.18E-3$	9.1	$2.56E-3$	22.9	$3.91E-2$	13.2	11.7
A1795	$3.03E-2$	5.2	$5.66E-3$	15.6	$4.47E-2$	15.4	13.4
A2199	$5.60E-2$	4.7	$2.37E-3$	24.5	$3.29E-2$	18.6	13.2
Late-type Galaxies							
A0779	$8.96E-6$	124.4	$5.29E-6$	208.0	$2.41E-4$	28.8	7.4
A1650	$4.38E-5$	119.6	$2.54E-5$	200.1	$2.09E-3$	17.0	6.9
A1795	$2.16E-3$	9.9	$2.90E-4$	32.9	$7.82E-3$	14.8	11.4
A2199	$4.12E-5$	105.8	$2.19E-5$	189.8	$1.20E-3$	26.7	8.1

Table 4: Morphological Parameters of the Clusters

Cluster	Γ_A (kpc)	Γ_B (kpc)	Θ_2 (deg)	ϵ
A0085	1358^{+52}_{-52}	868^{+53}_{-51}	154^{+5}_{-4}	$0.36^{+0.05}_{-0.05}$
A0779	1169^{+57}_{-55}	829^{+71}_{-65}	161^{+8}_{-8}	$0.29^{+0.06}_{-0.07}$
A1650	2162^{+85}_{-81}	1420^{+88}_{-88}	123^{+4}_{-4}	$0.34^{+0.05}_{-0.05}$
A1651	2119^{+75}_{-80}	1798^{+83}_{-76}	52^{+11}_{-12}	$0.15^{+0.05}_{-0.05}$
A1795	1365^{+69}_{-65}	1151^{+65}_{-61}	47^{+14}_{-16}	$0.16^{+0.06}_{-0.06}$
A1800	1084^{+57}_{-54}	910^{+63}_{-59}	63^{+18}_{-17}	$0.16^{+0.06}_{-0.06}$
A2034	1237^{+85}_{-82}	902^{+81}_{-87}	23^{+10}_{-10}	$0.27^{+0.09}_{-0.08}$
A2199	2182^{+53}_{-50}	1646^{+52}_{-46}	20^{+3}_{-3}	$0.25^{+0.03}_{-0.03}$
A2670	744^{+41}_{-41}	591^{+39}_{-37}	40^{+13}_{-10}	$0.21^{+0.07}_{-0.06}$
A2734	1413^{+62}_{-60}	1152^{+61}_{-57}	84^{+11}_{-9}	$0.18^{+0.05}_{-0.05}$

Table 5: Parameters for Testing the Presence of Substructure

Cluster	I	I_{90}	Skewness	clRej	Kurtosis	clRej	AI	clRej	TI	clRej	Δ_{obs}	$f(\Delta_{sim} > \Delta_{obs})$
A0085	1.03	1.03	−0.30	93.0	0.38	81.4	−0.22	31.0	1.18	96.8	251	0.304
A0779	1.09	1.04	0.08	35.6	0.84	95.2	−1.01	95.6	1.16	89.2	245	0.000
A1650	1.04	1.02	0.15	71.4	0.53	91.2	−0.43	58.6	1.21	99.2	326	0.156
A1651	1.05	1.02	−0.31	96.4	0.66	95.2	−0.61	77.4	0.99	7.2	345	0.075
A1795	0.96	1.03	−0.04	16.0	−0.34	51.4	−0.17	24.4	1.03	28.2	246	0.001
A1800	0.97	1.05	0.29	77.2	−0.54	66.6	0.87	90.6	0.87	84.0	118	0.034
A2034	0.95	1.06	0.18	53.0	−0.82	93.0	0.34	52.8	0.95	29.2	94	0.059
A2199	1.04	1.01	0.44	99.8	0.37	92.2	1.45	99.2	0.93	92.6	1456	0.000
A2670	0.94	1.05	−0.01	3.4	−0.66	86.0	−0.15	21.0	0.94	46.6	102	0.729
A2734	0.97	1.03	−0.07	29.4	−0.37	65.8	0.39	58.8	1.07	62.2	341	0.000

Table 6. Summary of Global Kinematic Properties for the Clusters

	Substructure?				Equilibrium?	
Cluster	1D	2D	3D	Morphology	X-Ray	v_{pec}
A0085	No	Yes	No	Elongated?	Yes	Yes
A0779	Yes	No	Yes	Elongated	No	...
A1650	Yes	Yes	No	Elongated	Yes	Yes
A1651	Yes	Yes	Yes	Spherical	Yes	No
A1795	No	No	Yes	Spherical	No	...
A1800	No	Yes	Yes	Spherical	Yes	...
A2034	No	No	Yes	Elongated	Yes	...
A2199	Yes	Yes	Yes	Elongated	Yes	...
A2670	No	Yes	No	Elongated	Yes	No
A2734	No	Yes	Yes	Spherical	Yes	...

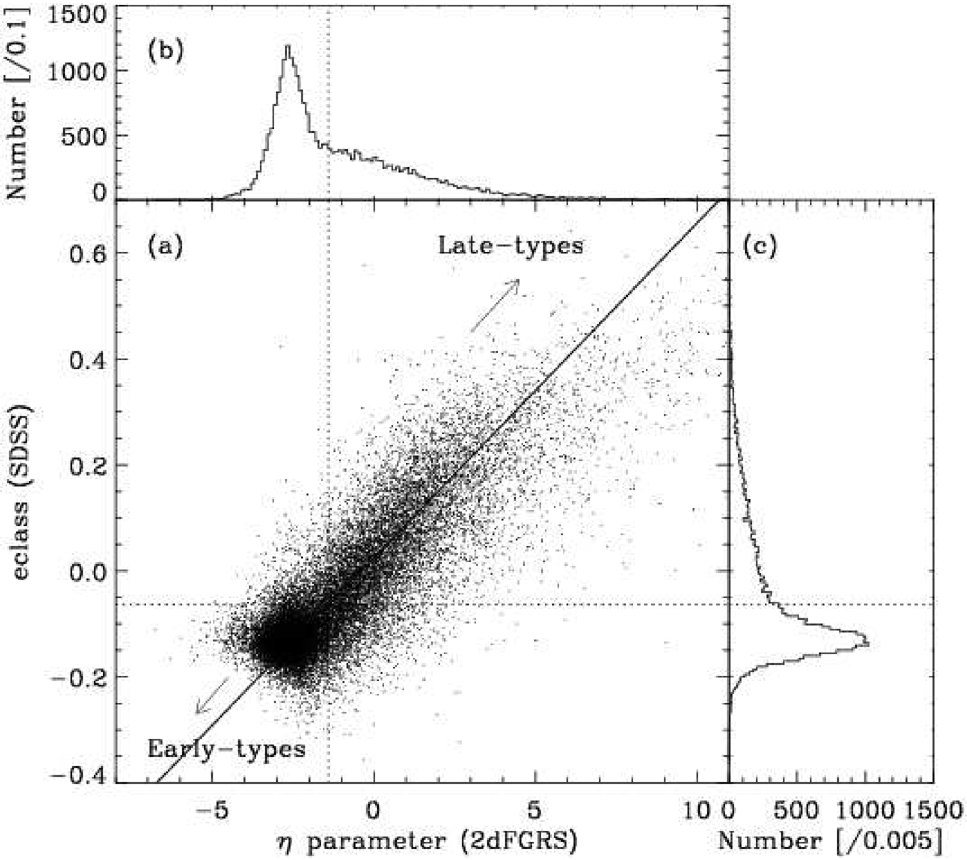

Fig. 1.— (a) Comparison of `eclass` parameter in SDSS with η parameter in 2dFGRS, (b) histogram for η parameter, and (c) histogram for `eclass` parameter. Solid line indicates the best linear fit for `eclass` (< 0.09) and η (< 1.1). The dotted vertical line denotes the division value $\eta = -1.4$ in 2dFGRS for galaxy subsamples, and dotted horizontal line indicates `eclass`$=-0.0640$ in SDSS, which is equivalent to the division value $\eta = -1.4$ in 2dFGRS.

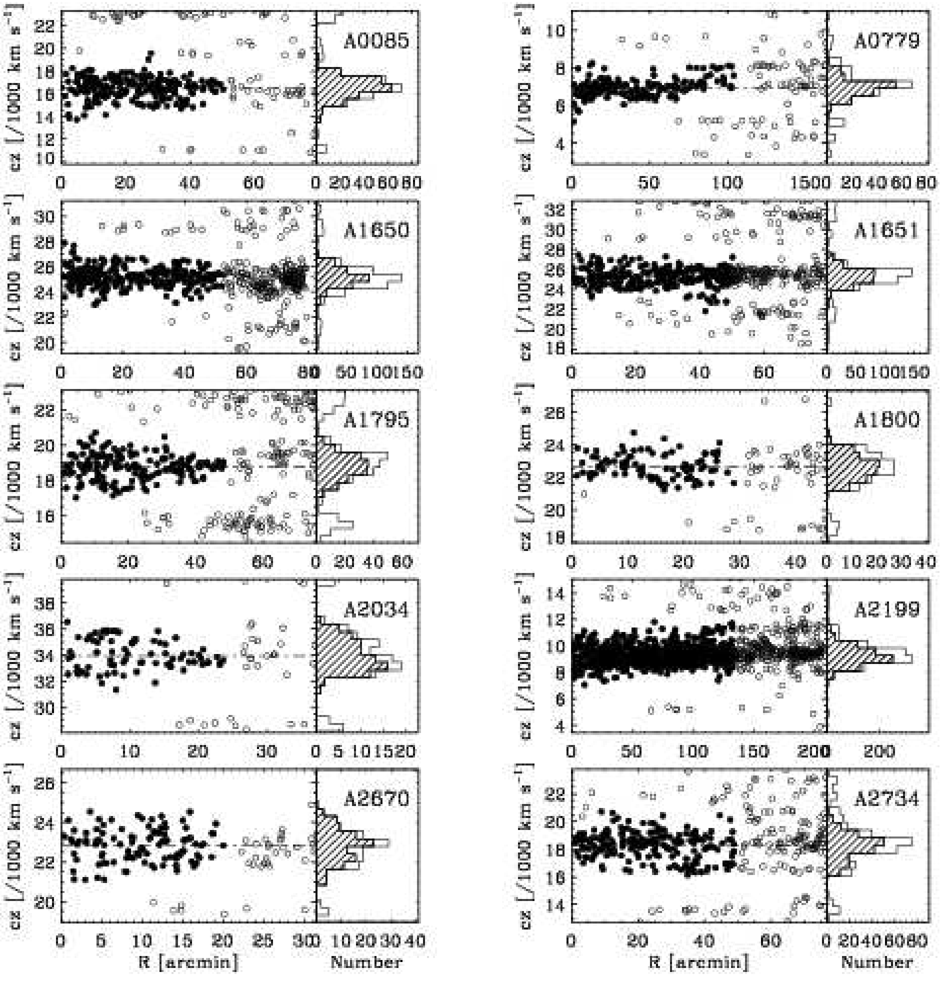

Fig. 2.— Radial velocity vs. clustercentric distance of galaxies and the velocity distribution for our sample clusters. Filled circles indicate the galaxies selected as cluster members, while open circles the galaxies not selected as cluster members. The horizontal dot-dashed lines indicate the systemic velocity of the clusters determined in Table 1. The velocity distributions for the member galaxies are shown by hatched histograms, and those for all of the observed galaxies by open histograms.

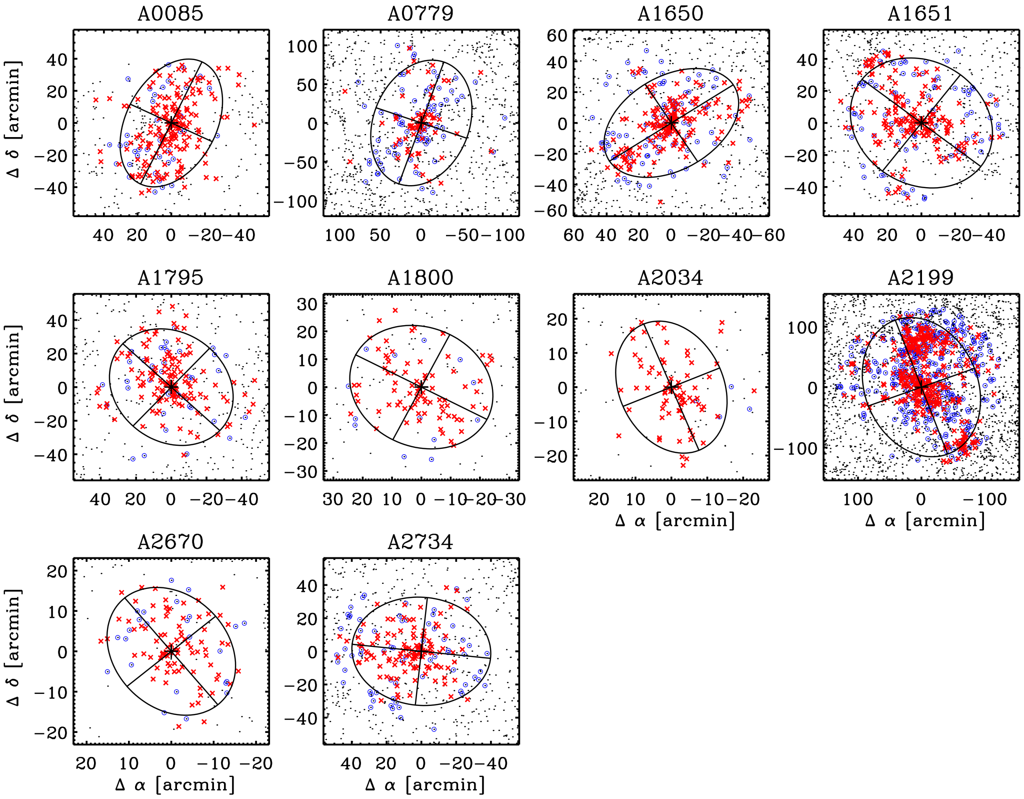

Fig. 3.— Spatial distribution of cluster galaxies with measured velocities for our sample clusters. Early-type galaxies are plotted with crosses, while late-type galaxies are with open circles. All the observed galaxies are represented by dots. The ellipses indicate the (twice enlarged) dispersion ellipse, and solid lines denote the major and minor axis of the dispersion ellipse.

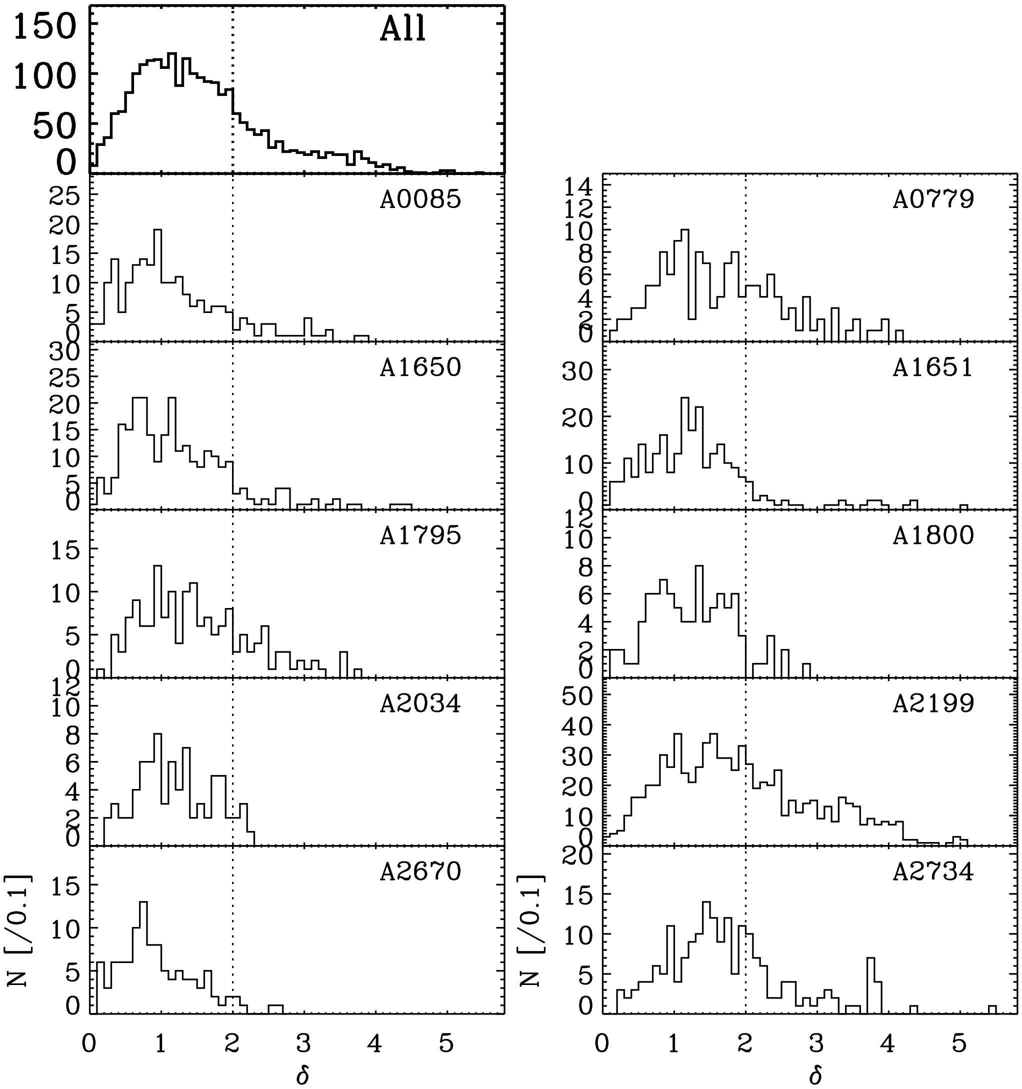

Fig. 4.— Distribution of the substructure parameter δ for our sample clusters. The dotted vertical lines indicate the selection criteria for the galaxies in the cluster main body.

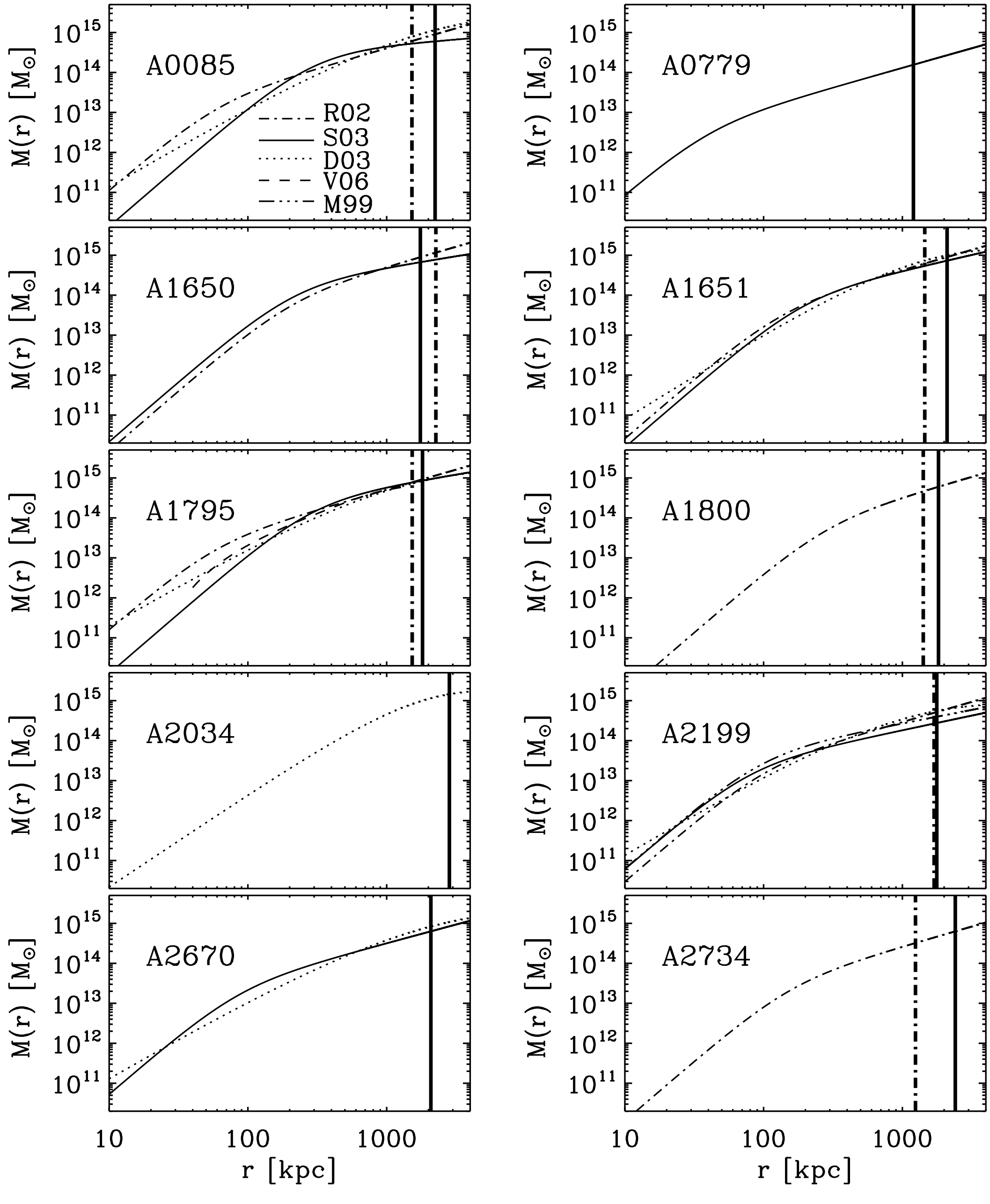

Fig. 5.— Total mass profiles for our sample clusters. Dot-dashed lines from Reiprich & Böhringer (2002, R02), solid lines are from Sanderson et al. (2003, S03), dotted lines from Demarco et al. (2003, D03), dashed lines from Vikhlinin et al. (2006, V06), and dot-dot-dashed lines from Markevitch et al. (1999, M99). The vertical dot-dashed and solid lines indicate the outer significance radius, r_X, in Reiprich & Böhringer (2002) and r_{200} radius computed in this study, respectively.

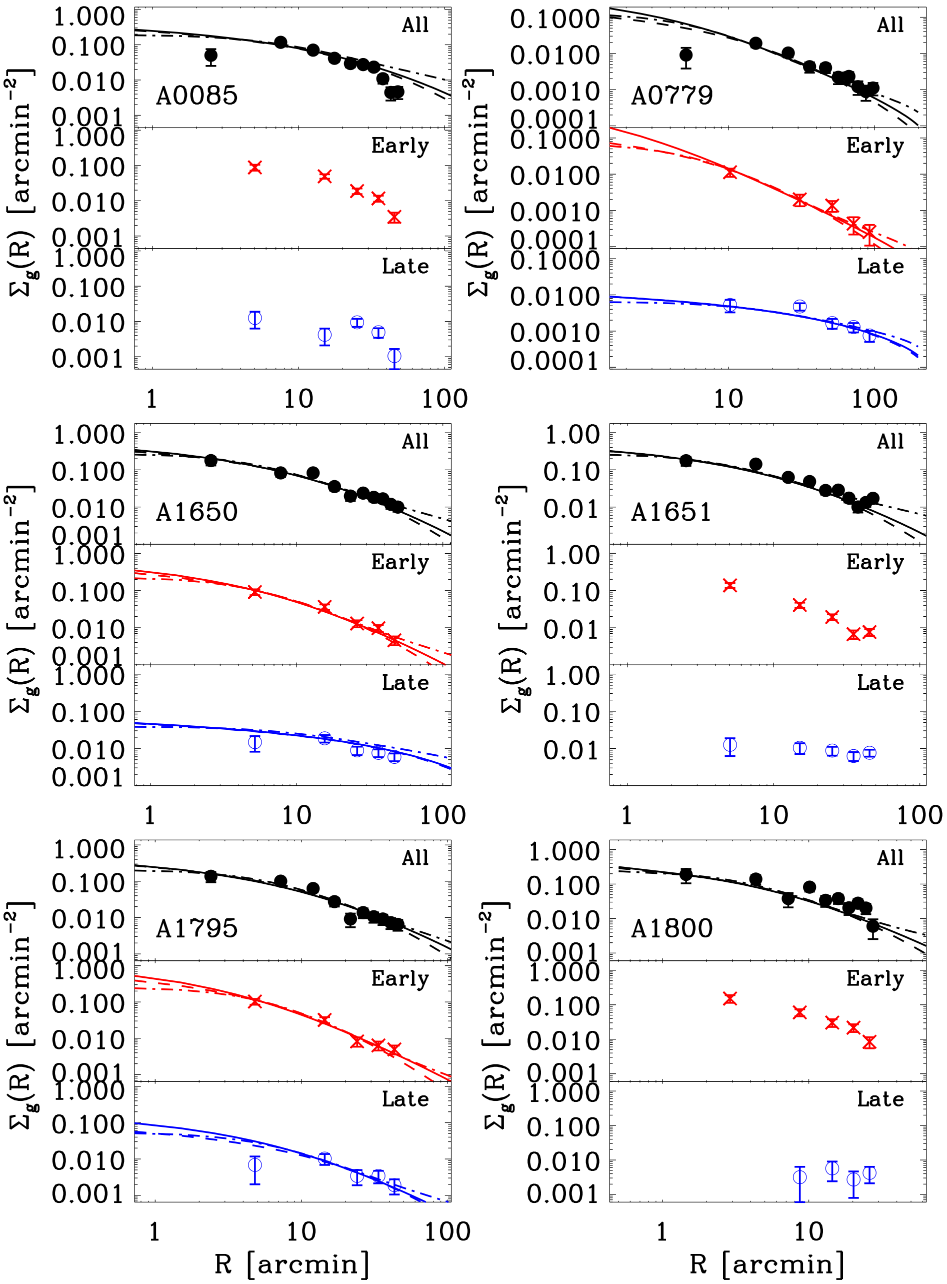

Fig. 6.— Projected number density profiles of all (top panel), early-type (middle panel), and late-type (bottom panel) galaxies with $\delta \leq 2.0$ for A85, 779, 1650, 1651, 1795, and 1800. The solid, dashed, and dot-dashed lines indicate the projection of the best fits using NFW, Hernquist, and KEK05 profiles, respectively, for each sample.

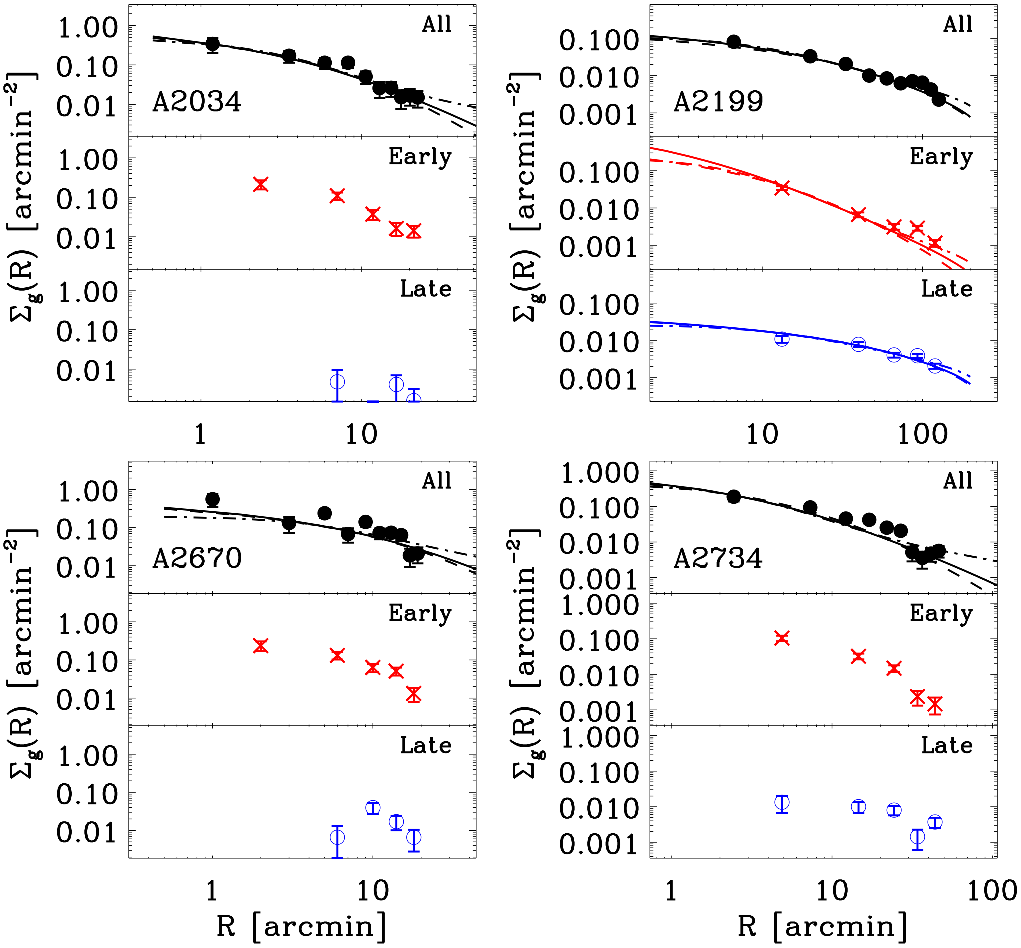

Fig. 7.— Same as Fig. 6, but for A2034, 2199, 2670, and 2734.

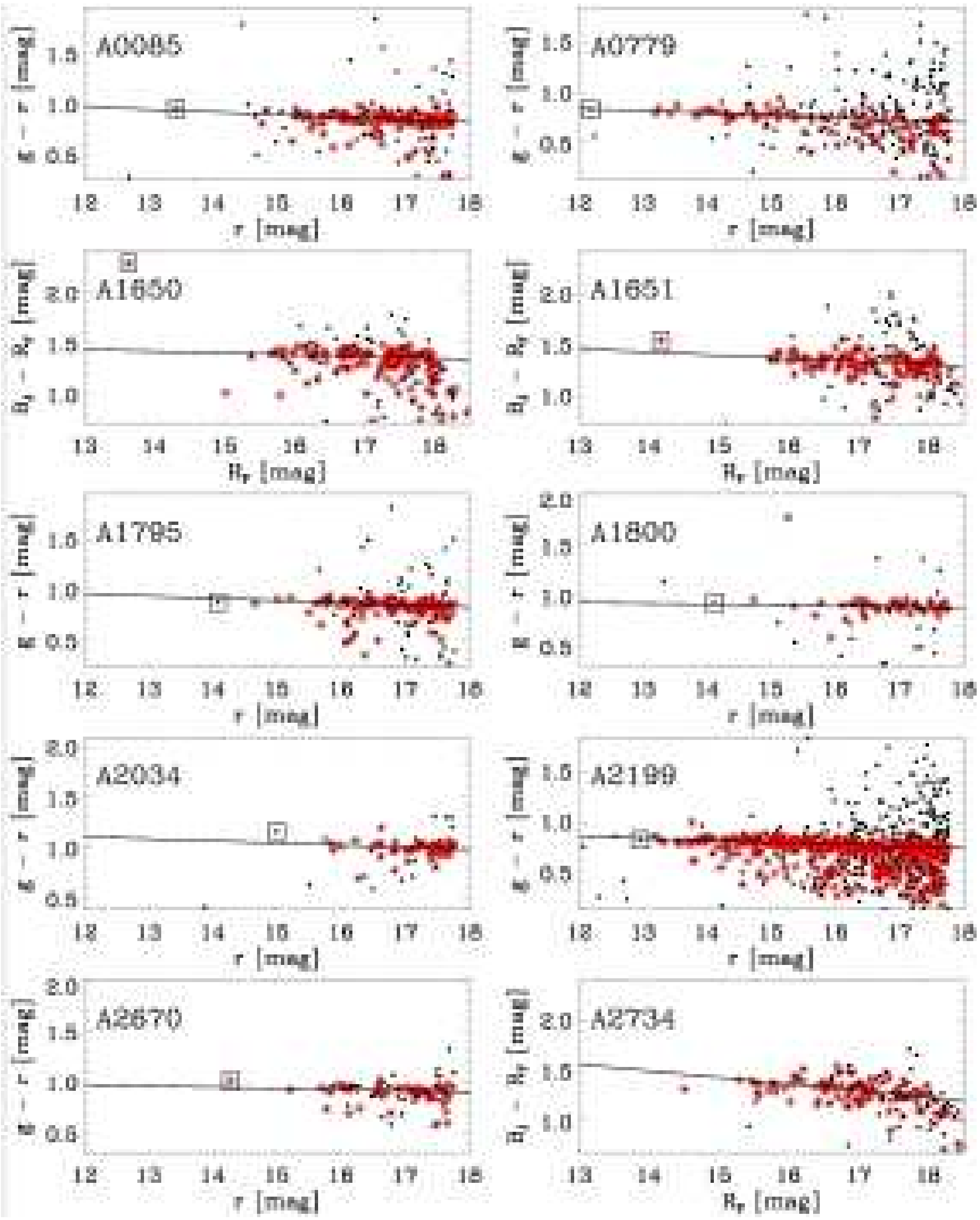

Fig. 8.— Color-magnitude diagrams for our sample clusters. Filled circles indicate the photometric sample of galaxies within the $R_{max}/2$ from the cluster center, while open circles the spectroscopically selected member galaxies in the same region. Solid lines indicate the best linear fit of the CMR for early-type galaxies. BCGs are marked by open squares.

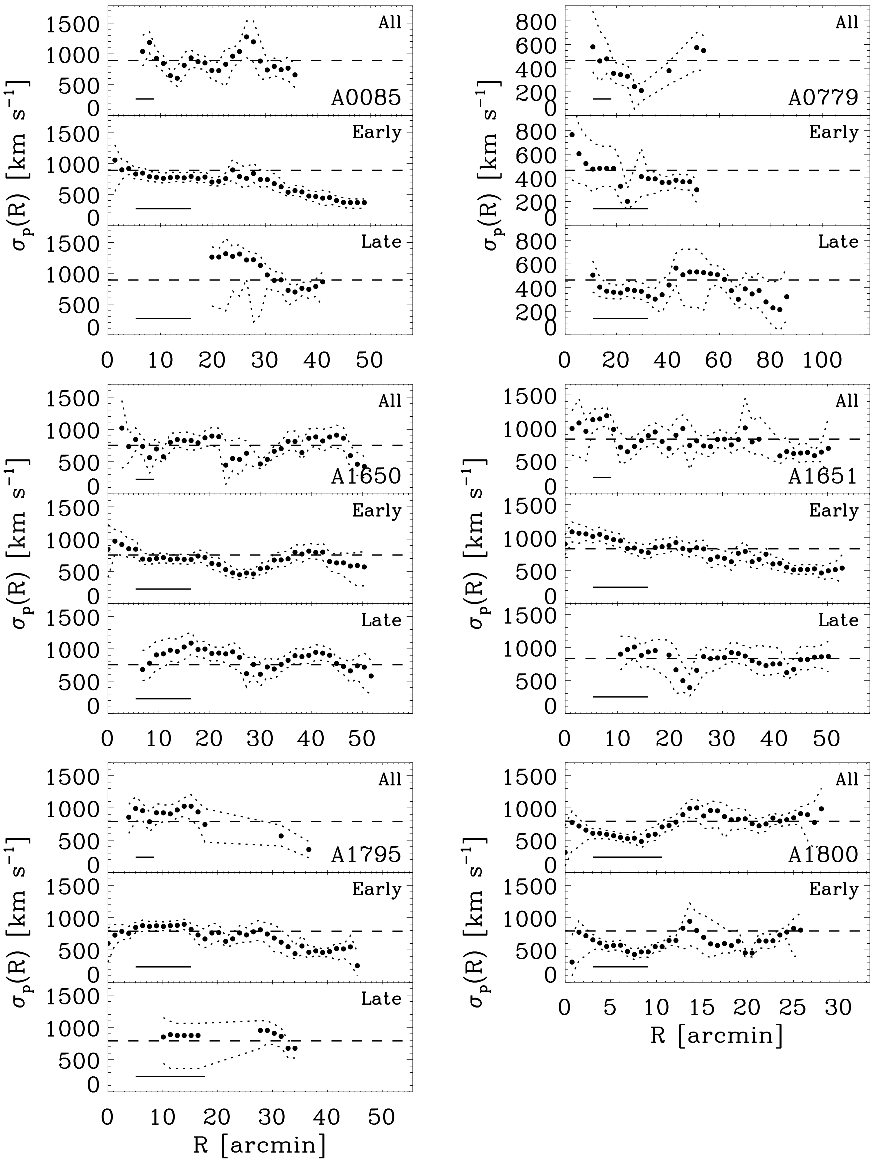

Fig. 9.— Velocity dispersion profiles of all (top panel), early-type (middle panel), and late-type (bottom panel) galaxies with $\delta \leq 2.0$ for A85, 779, 1650, 1651, 1795, and 1800. Filled circles indicate the velocity dispersion (σ_p) at each point. The dispersion is calculated using the galaxies within the moving radial bin that is represented by a horizontal errorbar in each panel. The dotted lines denote 68% confidence interval on the calculation of velocity dispersion. The dashed horizontal line indicates the global value of velocity dispersion using all galaxies in each cluster.

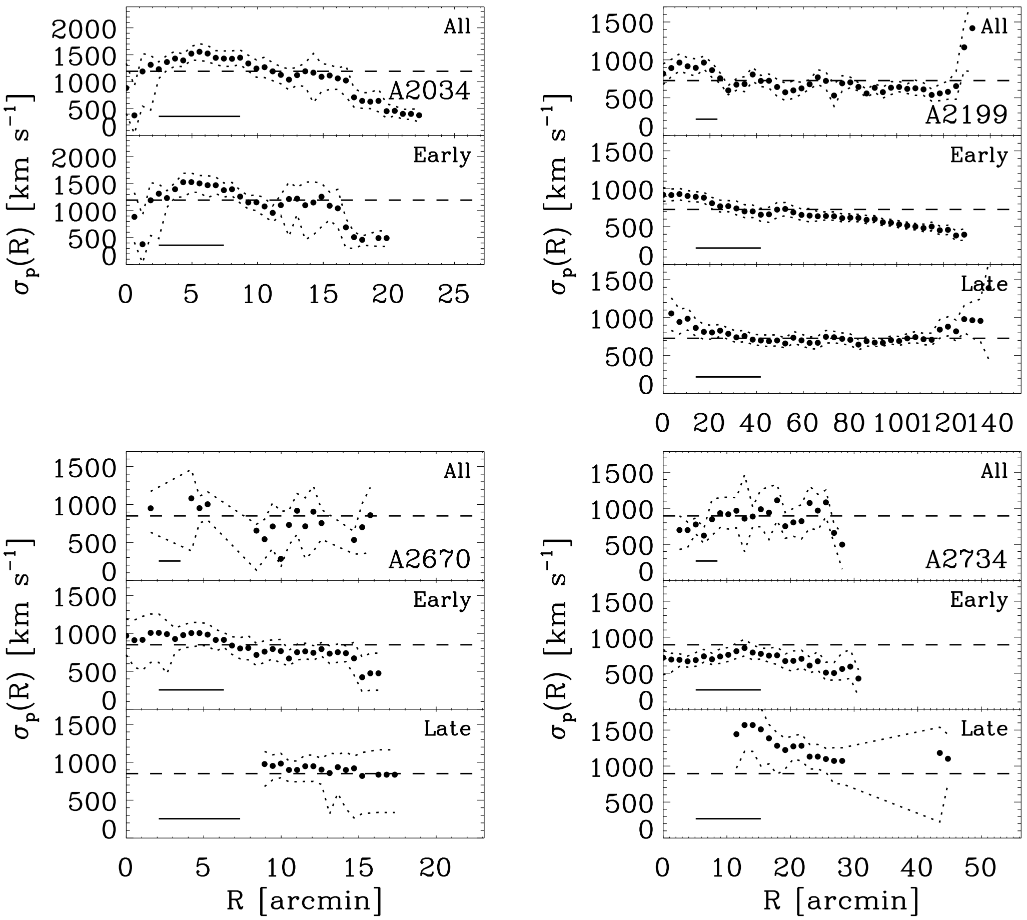

Fig. 10.— Same as Fig 9, but for A2034, 2199, 2670, and 2734.

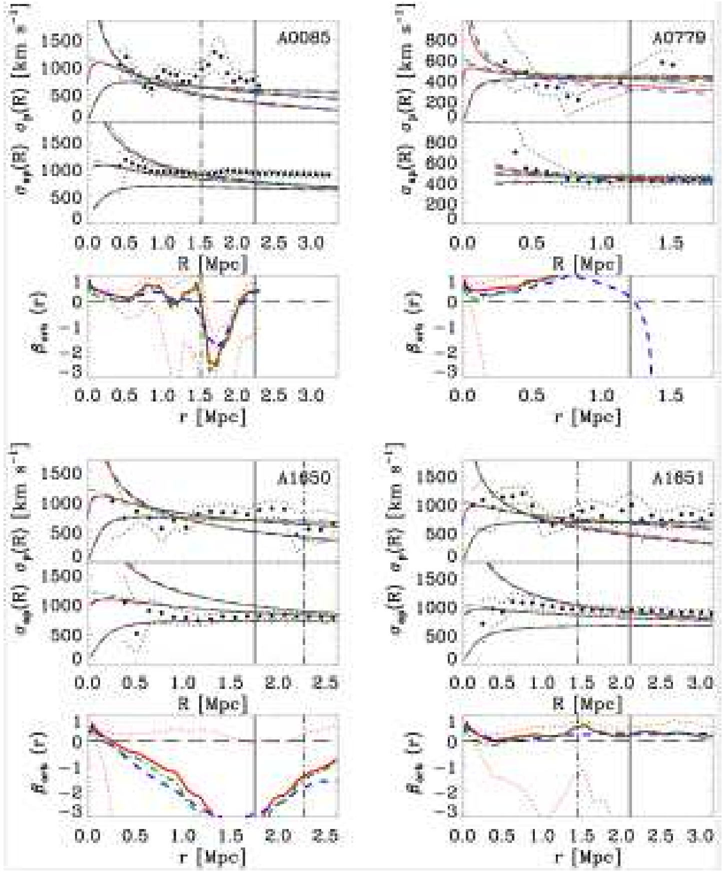

Fig. 11.— Velocity dispersion profile (top panel) and the aperture VDP (middle panel), velocity anisotropy profile (bottom panel) for all galaxies of A85, 779, 1650, and 1651. Filled circles in top panels represent the measured VDP shown in Fig. 9, and those in middle panel denote the measured aperture VDP. Associated, dotted lines represent 68% confidence interval on the calculation of velocity dispersion. Three smoothly curved lines in top and middle panels, from a radial anisotropy to the tangential one (from top to bottom, $\beta_{\rm orb}$= 0.99, 0, and −99), represent the calculated dispersion profiles using galaxy number density profile of NFW (solid lines), Hernquist (dashed lines), and KEK05 (dot-dashed lines). Velocity anisotropy profiles (VAPs) determined in §4.2 in the bottom panel are represented by solid (NFW), dashed (Herquinst), and dot-dashed line (KEK05). The errors of VAPs for NFW are shown by dotted lines. The vertical dot-dashed and solid lines indicate the outer significance radius, r_X, in Reiprich & Böhringer (2002) and r_{200} radius computed in this study, respectively.

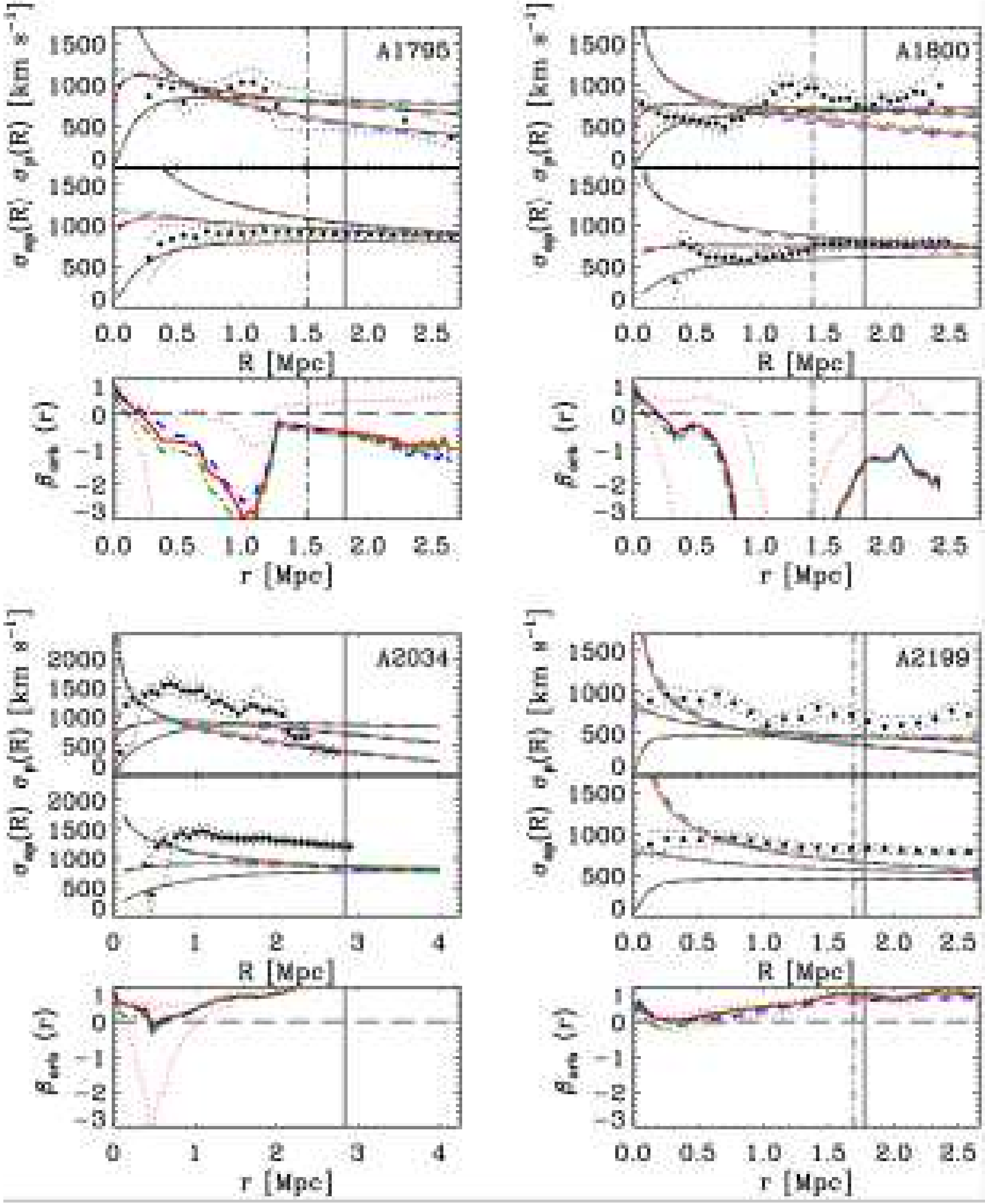

Fig. 12.— Same as Fig. 11, but for A1795, 1800, 2034, and 2199.

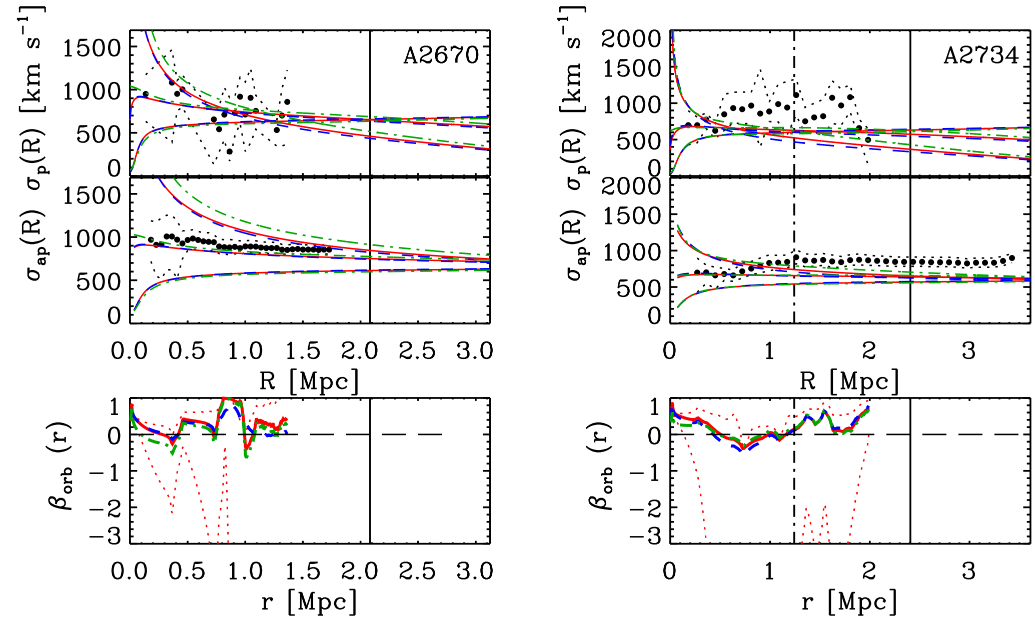

Fig. 13.— Same as Fig. 11, but for A2670 and A2734.

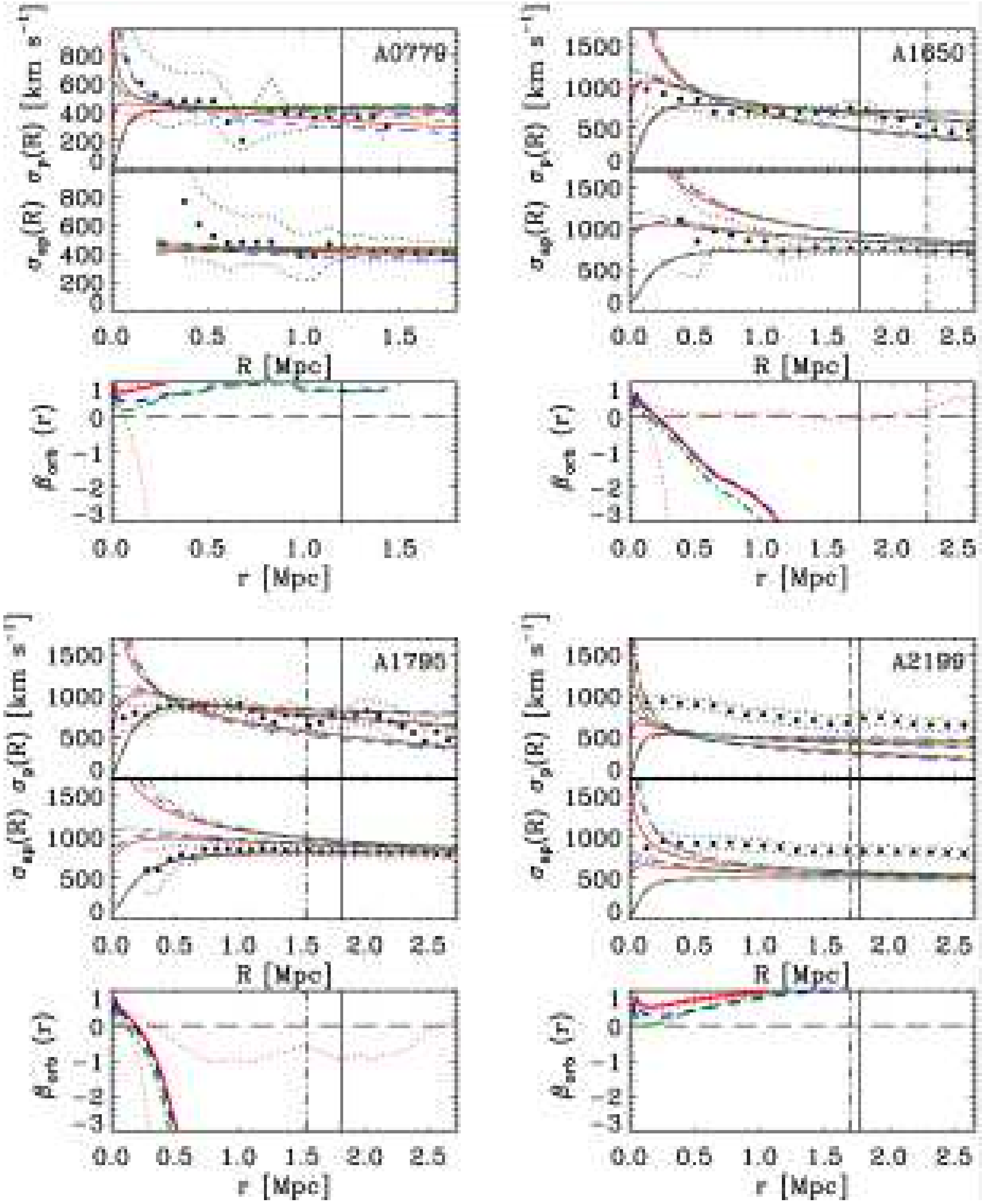

Fig. 14.— Same as Fig. 11, but for early-type galaxies in A779, 1650, 1795, and 2199.

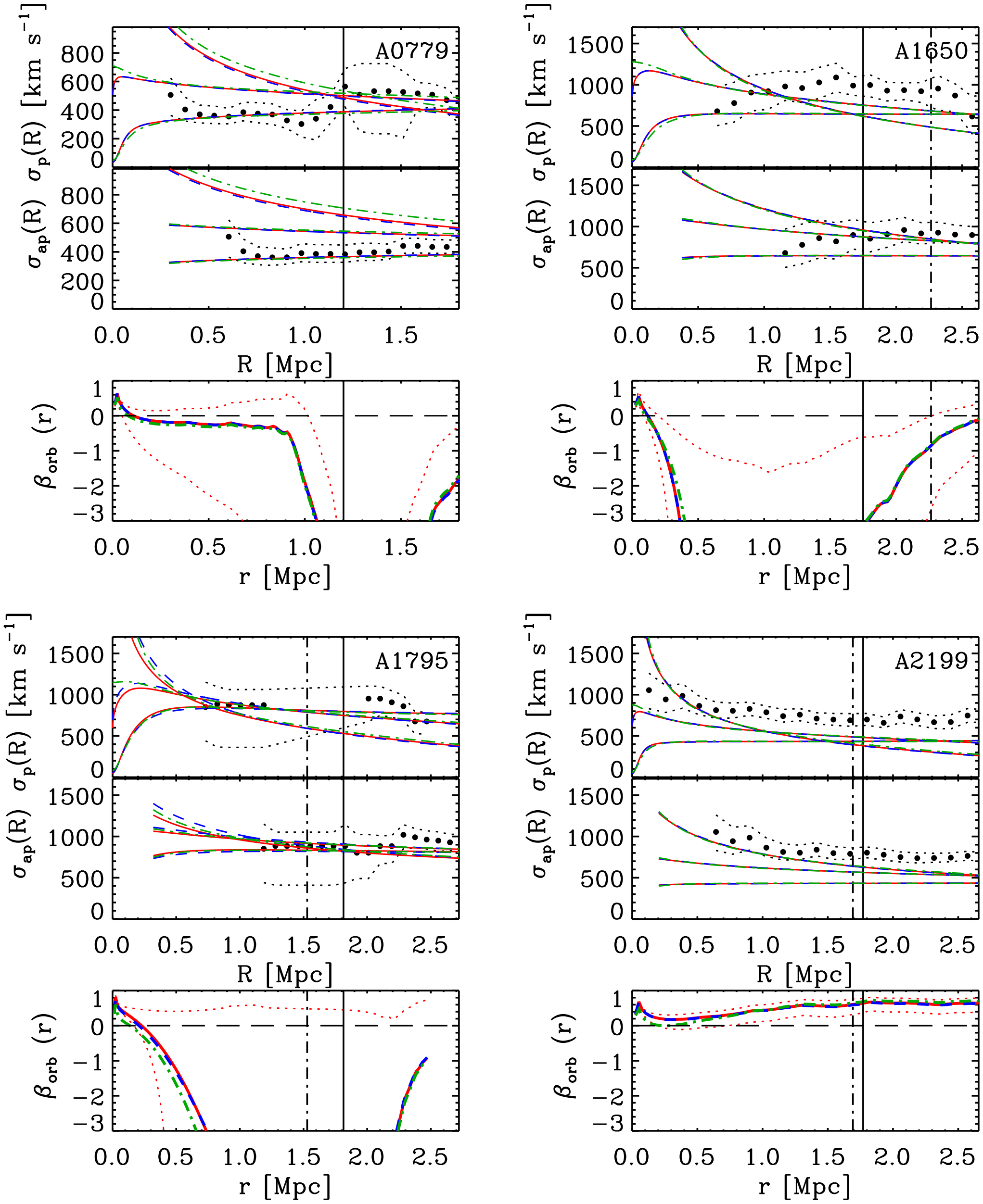

Fig. 15.— Same as Fig. 11, but for late-type galaxies in A779, 1650, 1795, and 2199.

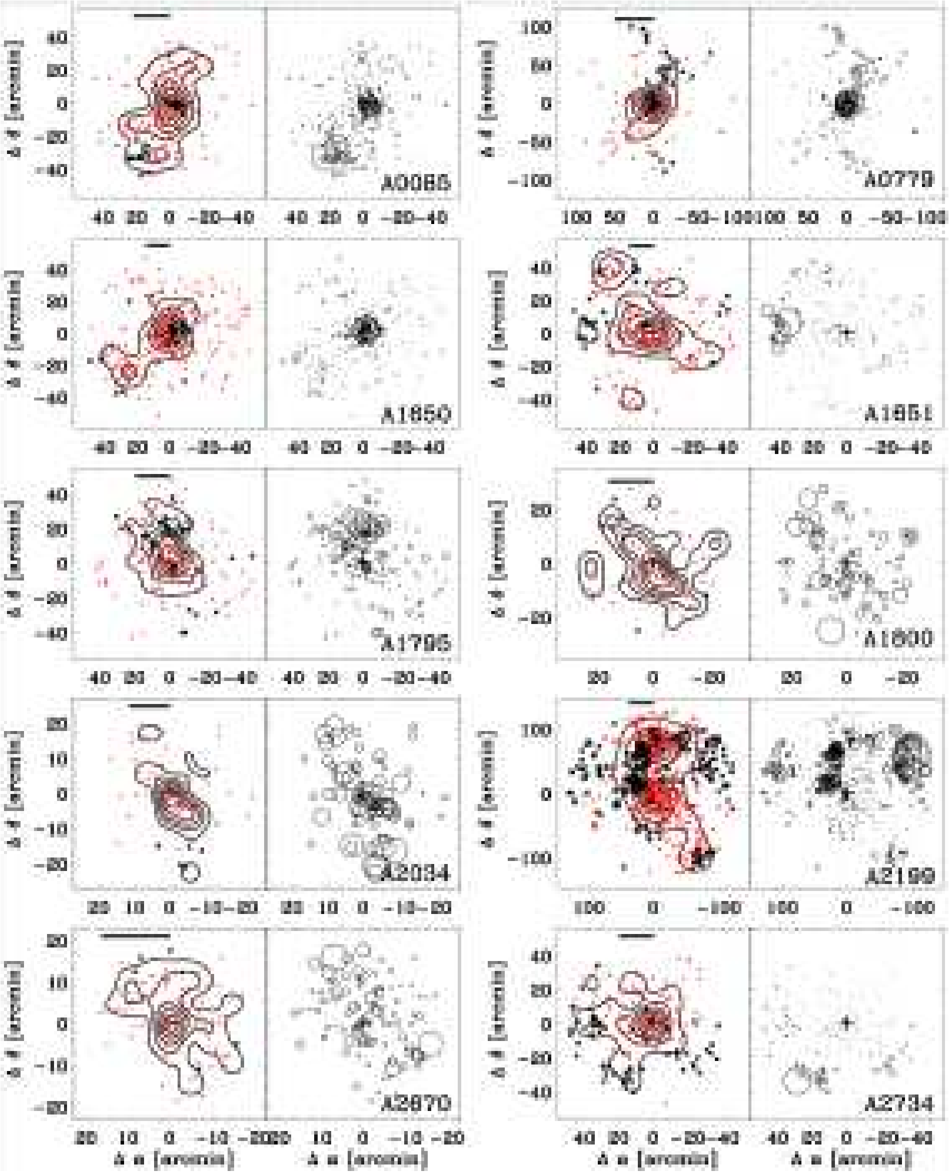

Fig. 16.— *Left panels*: Galaxy number density contour maps for our sample clusters. The member galaxies with $\delta \leq 2.0$ and $\delta > 2.0$ are represented by dots and crosses, respectively. The number density contours are overlaid. The plus signs indicate the cluster centroids, and the thick horizontal bars represent a physical extent of 1 Mpc. *Right panels*: Dressler-Shectman plots for the same clusters. Each galaxy is plotted by a circle with diameter proportional to e^{δ}. North is up, and east is to the left.

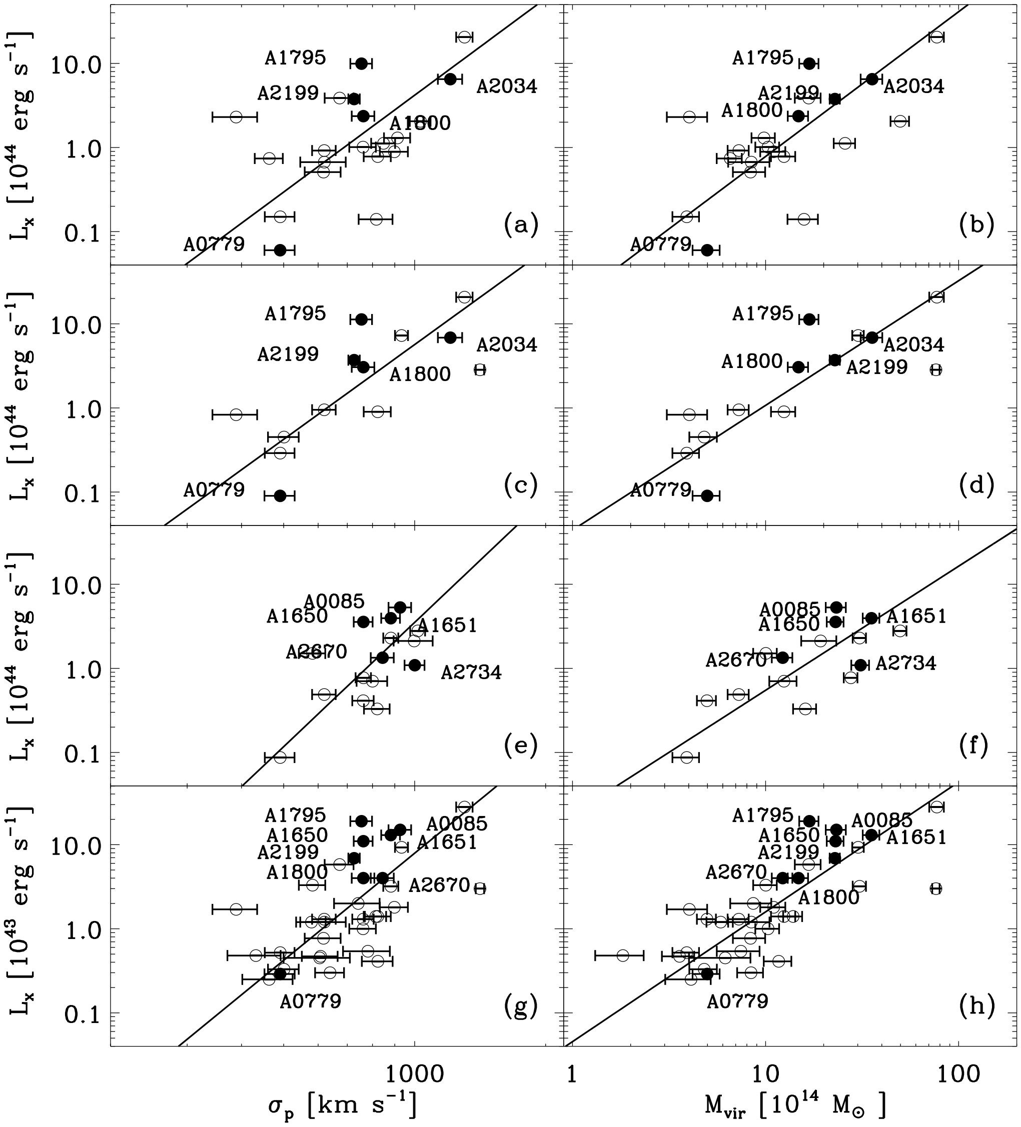

Fig. 17.— X-ray luminosity L_x (0.1−2.4 keV) vs. the velocity dispersion and virial mass for the our sample clusters (filled circles) compared with the other clusters (open circles) for the 113 selected clusters. X-ray luminosities in (a) and (b) are from Böhringer et al. (2000), those in (c) and (d) from Ebeling et al. (1998, 2000), those in (e) and (f) from Böhringer et al. (2004), and those (0.5−2.0 keV) in (g) and (h) from Ledlow et al. (2003). The solid lines indicate the best fit for each panel.

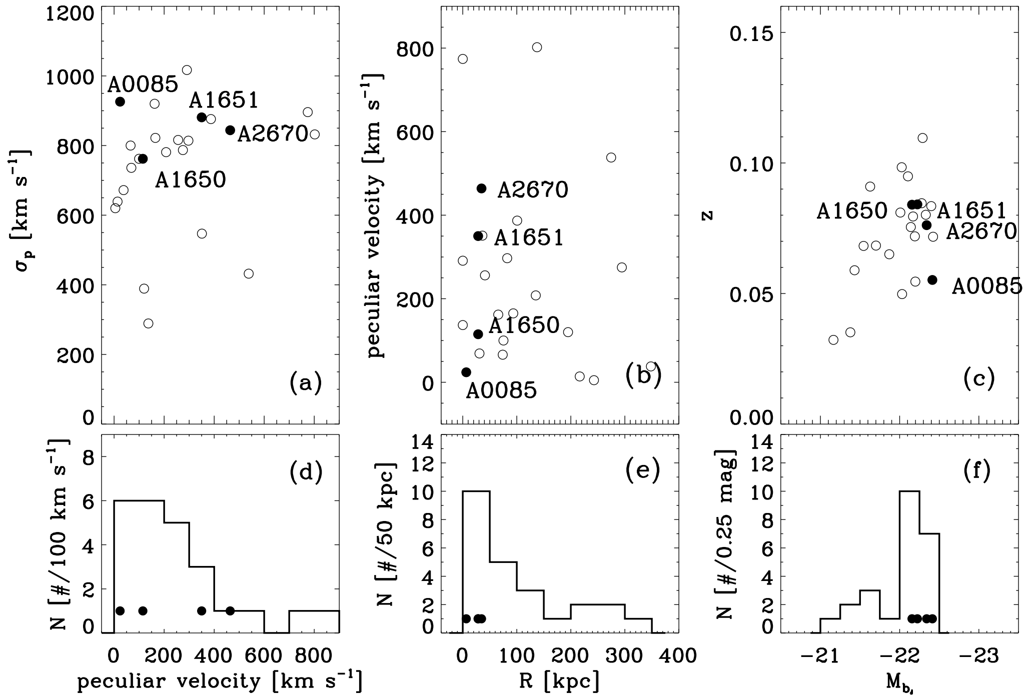

Fig. 18.— (a) Velocity dispersion as a function of the absolute value of the peculiar velocities of the BCGs, (b) absolute value of peculiar velocity as a function of the clustercentric distances of the BCGs, and (c) redshift as a function of the absolute magnitudes of the BCGs in the $b_{\rm J}$ band for our sample clusters (filled circles) compared with the other clusters (open circles) among the 113 selected galaxy clusters. Histograms of the peculiar velocities (d), the clustercentric distances (e), and the absolute magnitudes in the $b_{\rm J}$ band (f) of the BCGs are also shown for the clusters including our sample clusters. The clusters in our sample are marked by filled circles in (d), (e), and (f).

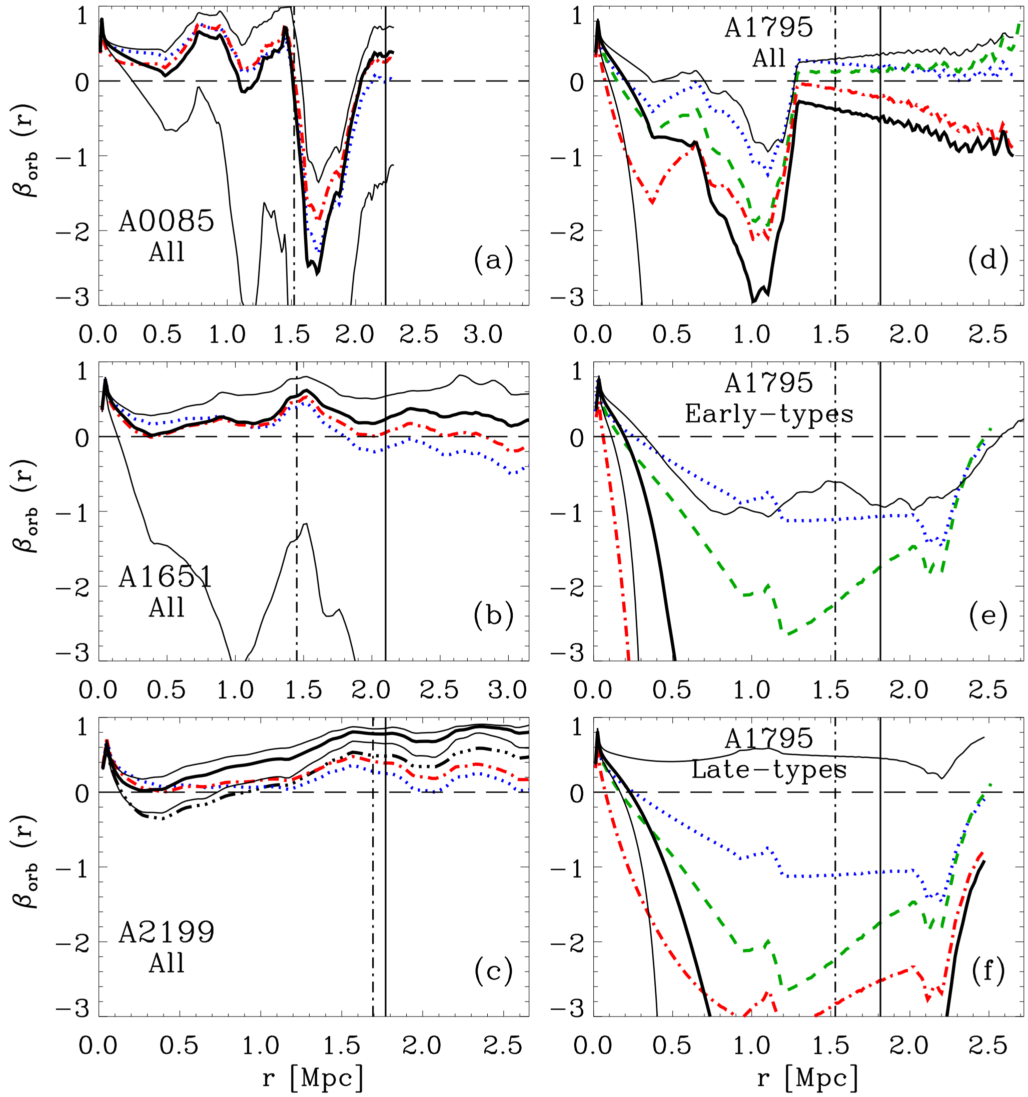

Fig. 19.— VAPs for all galaxies of A85 (a), A1651 (b), A2199 (c), and those for all (d), early-type (e), late-type galaxies (f) of A1795 determined in §4.2 using the NFW profile, but based on several mass profiles: Sanderson et al. (2003, thick solid), Demarco et al. (2003, thick dotted), Reiprich & Böhringer (2002, thick dot-dashed), Markevitch et al. (1999, thick dot-dot-dashed), and Vikhlinin et al. (2006, thick dashed). The errors of VAPs using the mass profile of Sanderson et al. (2003) are shown by thin solid lines. The vertical dot-dashed and solid lines indicate the outer significance radius, r_X, in Reiprich & Böhringer (2002) and r_{200} radius computed in this study, respectively.

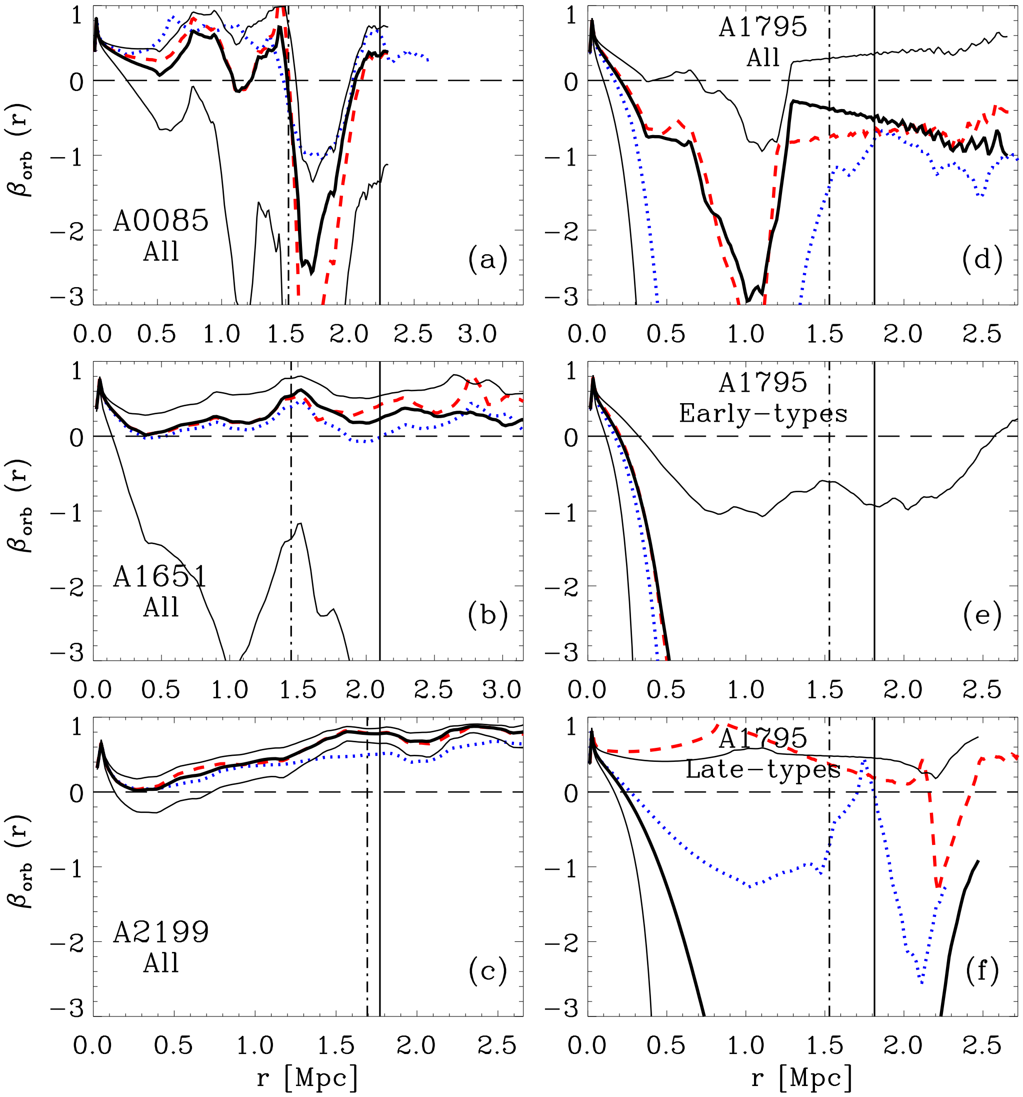

Fig. 20.— VAPs for all galaxies of A85 (a), A1651 (b), A2199 (c), and those for all (d), early-type (e), late-type galaxies (f) of A1795 determined in §4.2 using the NFW profile, but based on several galaxy samples: galaxies with $\delta \leq 2.0$ (thick solid), galaxies with $\delta \leq 1.8$ (thick dashed), and galaxies with $\delta \geq 0$ (thick dotted). The errors of VAPs based on the galaxies with $\delta \leq 2.0$ are shown by thin solid lines. The vertical dot-dashed and solid lines indicate the outer significance radius, r_X, in Reiprich & Böhringer (2002) and r_{200} radius computed in this study, respectively.

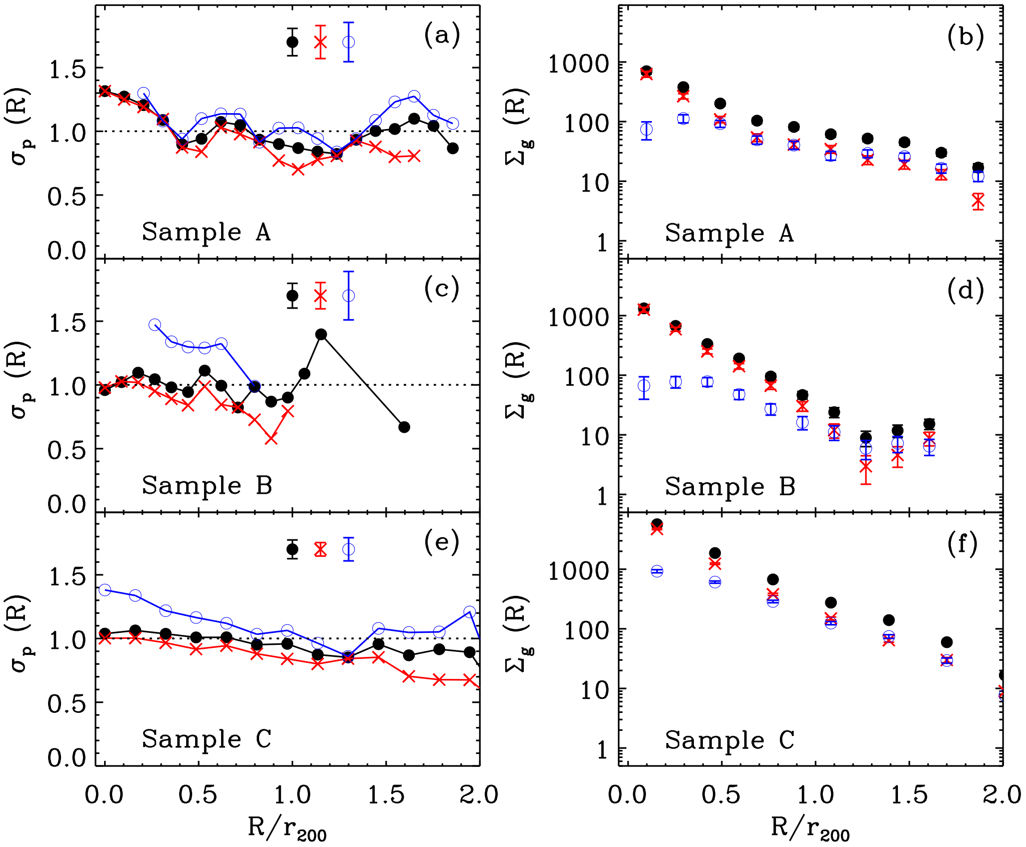

Fig. 21.— (a) VDPs and (b) projected galaxy number density profiles for the clusters in Sample A; (c,d) those in Sample B; and (e,f) those in Sample C. Filled circles, crosses, and open circles denote all, early-type, and late-type galaxies, respectively. Typical errors of dispersion profiles are shown by errorbars according to the subsamples.